Meteorologische Zeitschrift, Vol. **21**, No. 6, 531–550 (December 2012)

Open Access Article

Weather patterns and hydro-climatological precursors of extreme floods in Switzerland since 1868

PETER STUCKI[1,*], RALPH RICKLI[1], STEFAN BRÖNNIMANN[1,2], OLIVIA MARTIUS[1,2], HEINZ WANNER[1,2], DIETMAR GREBNER[3] and JÜRG LUTERBACHER[4]

[1]Institute of Geography, University of Bern, Switzerland
[2]Oeschger Centre, University of Bern, Switzerland
[3]Institute for Atmospheric and Climate Science, ETH Zurich, Switzerland
[4]Department of Geography, Justus-Liebig-University Giessen, Germany

(Manuscript received February 21, 2012; in revised form October 30, 2012; accepted October 31, 2012)

Abstract

The generation of 24 extreme floods in large catchments of the central Alps is analyzed from instrumental and documentary data, newly digitized observations of precipitation (DigiHom) and 20th Century Reanalysis (20CR) data. Extreme floods are determined by the 95th percentile of differences between an annual flood and a defined contemporary flood. For a selection of six events between 1868 and 1910, we describe preconditioning elements such as precipitation, temperature, and snow cover anomalies. Specific weather patterns are assessed through a subjective analysis of three-dimensional atmospheric circulation. A focus is placed on synoptic-scale features including mid-tropospheric ascent, low-level moisture transport, propagation of cyclones, and temperature anomalies. We propose a hydro-meteorological classification of all 24 investigated events according to flood-generating weather conditions. Key elements of the upper-level synoptic-scale flow are summarized by five types: (i) pivoting cut-off lows, (ii) elongated cut-off lows, (iii) elongated troughs, (iv) waves (with a kink), and (v) approximately zonal flow over the Alpine region. We found that the most extreme floods (as above, but $\geq$ 98th percentile) in Switzerland since 1868 were caused by the interaction of severe hydro-climatologic conditions with a flood-inducing weather situation. The 20CR data provide plausible synoptic-scale meteorological patterns leading to heavy precipitation. The proposed catalogue of weather patterns and hydro-climatologic precursors can give direction when anticipating the possibility of severe floods in the Alpine region.

Keywords: extreme flood events, central alps, switzerland, hydro-meteorological, climatological case studies, weather pattern classification, atmospheric precursors, extreme hochwasserereignisse, schweiz, alpen, fallstudien, wetter muster klassifikation.

1 Introduction

The Alpine region is sensitive to floods due to the frequent occurrence of heavy precipitation, the potential contribution of snowmelt, and mesoscale dynamics (FREI et al., 2000; WEINGARTNER et al., 2003; FREI and SCHMIDLI, 2006). Recent floods in the Swiss Alps, such as the catastrophic event in August of 2005, have caused fatalities and damaged infrastructure (BEZZOLA et al., 2008). Since 1987, Swiss federal authorities have explored the hydrological and meteorological characteristics of floods (e.g., ASCHWANDEN, 2000; BEZZOLA and HEGG, 2007, 2008).

Compared to recent years, few floods occurred between 1950 and 1987 (PFISTER, 2009), the time covered by reanalysis data sets. Hydrological and meteorological conditions of floods prior to 1950 have been studied using historical data (RÖTHLISBERGER, 1991; PFISTER, 1999; WANNER et al., 2004; SCHMOCKER-FACKEL and NAEF, 2010; WETTER et al., 2011), and compared to more recent events (PETRASCHECK, 1989; FREI, 2005). In Switzerland, a rich body of historical literature on floods is available (e.g., COAZ, 1869; BILLWILLER, 1876). Supplemented with quantitative information (e.g., from the Annals of the Schweizerische Meteorologische Zentralanstalt; ASMA), the classification of Alpine floods is possible. For instance, SCHMOCKER-FACKEL and NAEF (2010) distinguished North-East, North-West, and South types regarding the hydrological extent of flood events (see also HILKER et al., 2008). Other studies have investigated the weather regimes associated with floods. Historical winter floods in Central Europe were associated with southward displaced zonal circulation belts or southwesterly inflow on a monthly scale (STURM et al., 2001; JACOBEIT et al., 2003). Summer floods in Central Europe since 1948 were mainly ascribed to a cut-off low from the Icelandic trough moving to the northern Mediterranean and following the van Bebbers cyclone track Vb (JACOBEIT et al., 2006). BARDOSSY and FILIZ (2005)

*Correspondence address: Peter Stucki, Climatology Research Group, Institute of Geography, University of Bern, Hallerstrasse 12, 3012 Bern, Switzerland. E-mail: peter.stucki@giub.unibe.ch

DOI 10.1127/0941-2948/2012/368

0941-2948/2012/368 $ 9.00

associated negative anomalies in sea level pressure (SLP) patterns over the Bay of Biscay or the western Mediterranean (positive anomalies from the eastern Mediterranean to Russia) with summer floods in pre-Alpine regions.

For Swiss catchments, there is substantial knowledge about regimes producing heavy precipitation, but not specifically about flood-causing weather. WEHRY (1967) identified five weather situations responsible for precipitation rates of $\geq$ 50 mm/$\geq$ 2500 km^2/day . GREBNER and ROESCH (1998) proposed six circulation patterns responsible for (primarily cyclonic generation of) heavy precipitation in Switzerland from 1977 to 1993. One example is cyclonic cold air advection towards the Alps from the northwest combined with advection of warm air from the south or southeast by a secondary vortex. Other typical atmospheric conditions associated with sustained precipitation along the southern slope of the Alps (AS) are specified in MARTIUS et al. (2006). These include a conditionally unstable environment, advection of moist low-level air masses, and an orographically forced ascent (e.g., DOSWELL et al., 1996; MASSACAND et al., 1998, HOINKA et al., 2006; BOUDEVILLAIN et al., 2009).

In this study, we use novel meteorological data sets which allow a detailed quantitative analysis of precipitation and atmospheric circulation preceding and during major floods between 1868 and 1910. During this period, floods were comparatively frequent (PFISTER, 1999; SCHMOCKER-FACKEL and NAEF, 2010). These data sets include daily precipitation observations from weather stations in Switzerland (BEGERT et al., 2005; FÜLLEMANN et al., 2011) as well as a global, three-dimensional reanalysis (COMPO et al., 2011). We supplement these data sets with hydrological and climatological information to explore the main contributors to floods (e.g., heavy precipitation events and their synoptic/temporal characteristics) and antecedent hydro-climatological elements such as soil moisture, snow accumulation, and temperature (DOSWELL et al., 1996; WEINGARTNER et al., 2003; WANNER et al., 2004; MARKOWSKI and RICHARDSON, 2010). We present examples of extreme floods in four Swiss catchments since 1868. Our assessment considers hydrological, climatological, and meteorological perspectives. First, we analyze preconditioning factors, i.e., the hydro-climatological disposition, since the winter preceding the event (“long-term”). Then, we explore the “short-term” (i.e., lasting from a few hours to several days) hydrological triggers (i.e., the initiation of high discharges by heavy precipitation) and the meteorological triggering (i.e., the activation of heavy precipitation by weather systems). Finally, we address the maintaining factors, i.e., the meteorological factors contributing to the maintenance of heavy precipitation over several days (cf. JACOBEIT et al., 2006).

All studied events are then classified according to the synoptic-scale flow configuration which accompanied the flood-triggering heavy precipitation event. Additionally, we discuss the relationship between synoptic and smaller-scale dynamics in the Supplement (available online on the journals website at www.schweizerbart.de/journals/metz).

2 Data

2.1 Lake level and runoff data

We explore lake level data from Lake Constance (Constance; available since 1817) and Lake Zurich (Zurich; available since 1811) on the northern slope of the Alps (AN), and Lago Maggiore (Locarno; available since 1869) on the southern slope of the Alps (AS). Lake level data for Lago Maggiore and Lake Zurich were supplied by the Swiss Federal Office for the Environment (FOEN, Hydrology Division; accessed in June 2009). Lake level data for Lake Constance were provided by the German Landesanstalt für Umwelt, Messungen und Naturschutz Baden-Württemberg (LUBW; accessed in June 2009). We also consider data from the Rhine River (Rheinhalle near Basel; available since 1869; FOEN). The Rhine drains the largest area of Switzerland north of the Alps (see Fig. 1). Daily mean discharges and daily gauge readings (MQd), as well as annual floods and flood levels (HQa) are used as base parameters.

2.2 Meteorological surface data

We use daily precipitation sums (5:40 AM to 5:40 AM of the next day in mm) at Swiss weather stations (provided by MeteoSwiss). Some series reach back to 1864. This is supplemented with precipitation data from COAZ (1869) and BILLWILLER (1876). For the flood in 1868, recordings from 32 stations are available. For the flood in 1951, data from 287 stations are available. Thirteen of the precipitation data series have been homogenized (BEGERT et al., 2005). Since our study is limited to several well-documented events, we can manually assess outliers. Furthermore, we value short-term dynamics over climatological stability. For instance, we are interested in day-to-day shifts of temperature or precipitation fields during a flood event. Therefore, a good spatial coverage by meteorological data is preferred over homogeneity in the station series.

In addition to the Swiss data, we have daily resolved precipitation data from neighboring countries (ECAD data set; KLEIN TANK et al., 2002). Mean seasonal or monthly temperature and precipitation amounts for individual stations were calculated for the 1961–1990 period according to BEGERT et al. (2007).

2.3 Reanalysis data

This study considers the Twentieth Century Reanalysis version 2 (20CR; COMPO et al., 2011). This global scale, six hour resolved, and three-dimensional atmospheric dataset goes back to 1871. 20CR is based on an ensemble Kalman filter assimilation of surface and SLP

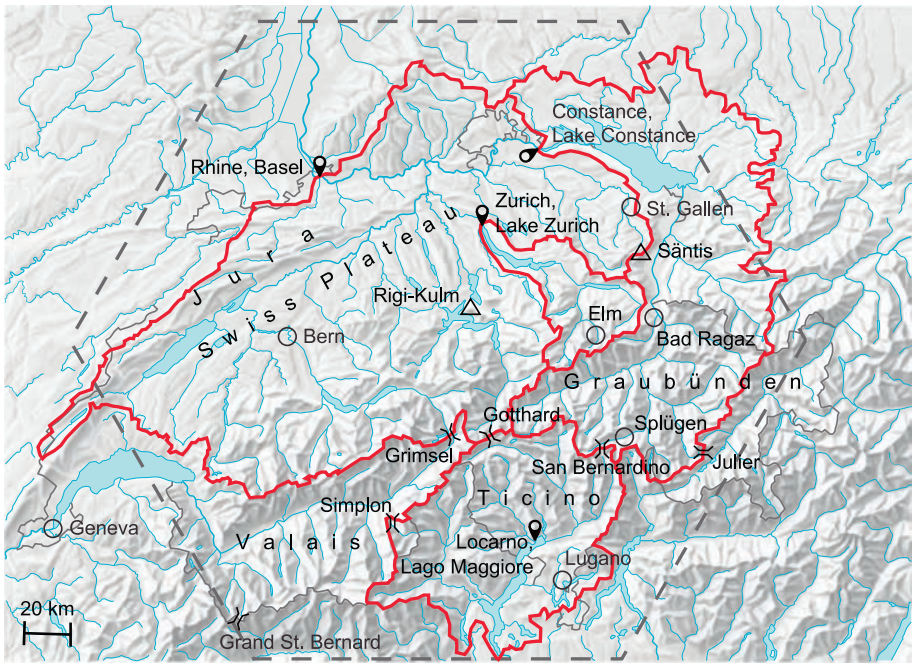

Figure 1: Topographic relief and waterways in relevant region of Switzerland (base map courtesy of swisstopo). Selected gauge stations (denoted with cones) are located within the corresponding catchment (denoted with a red line). Frequently mentioned geographical regions (spaced letters) and locations such as localities (circles), mountain passes (bridge symbols), and summits (triangles) are indicated. A dashed grey hexagon demarcates areas exposed to damage and intense precipitation (see Table 1).

observations. Monthly mean sea surface temperatures (SST) and sea ice concentrations serve as boundary conditions. An experimental version of the US National Center for Environmental Prediction/Global Forecast System (NCEP/GFS) atmosphere/land model from 2008 is used at a resolution of T62 in the horizontal and 28 hybrid sigma-pressure levels in the vertical. In this paper, we consider an ensemble mean of 56 members. For the 1868 event, an experimental back-extension using the 20CR system and surface pressure input from the ISPDv2 data base was utilized, but with the following changes: no tropical cyclone data were assimilated and SST and sea ice are the monthly 1871–1900 average. Because the convex 20CR model orography representing the Alps reaches only ca. 1000 m a.s.l. (see the Fig. 1 Supplement) terrain-induced effects (e.g., orographic lifting or flow convergence) are likely to be underrepresented.

The potential and limitations of 20CR for various applications has been scrutinized (e.g., in terms of trend analyses; FERGUSON and VILLARINI, 2012). However, 20CR has been shown to accurately represent synoptic-scale features related to individual storms (BRÖNNIMANN et al., 2012). The dense observational data sets in this study provide insight into the use of 20CR for exploring heavy precipitation events in complex topography. Analyses of the ensemble standard deviations for the events in 1876 and 1993, respectively, show that over much of the continent and for most of the variables used here, they are sufficiently small for the purpose of this study. Nevertheless, they can be up to twice as large in the 1876 case compared to 1993 (e.g., in the range of 2 hPa and 1 hPa for SLP; not shown). The limitations of global models in accurate representation of precipitation are reflected in the comparatively low precipitation rates. In addition, the ensemble standard deviations are larger for both events, reaching approximately 0.8 mm/h at mean rates of $\leq$ 2.5 mm/h. The spatial patterns of precipitation rates are less affected. For more recent events, 20CR was also compared to NCEP/NCAR Reanalysis (KALNAY et al., 1996; KISTLER et al., 2001), GFS Analysis, BOLAM3 (BUZZI and FOSCHINI, 2000), the EMULATE data set (ANSELL et al., 2006), and meteorological maps (e.g., GREBNER and RICHTER, 1991; GREBNER, 1993; CASSARDO et al., 2001). Consistency was found in the spatio-temporal representation of meteorological variables and only 20CR is shown in this study.

2.4 Data from historical reports and literature

The numerical data are supplemented with information from historical reports, bulletins, or literature (e.g., ASMA; COAZ, 1869; BILLWILLER, 1876; AMBROSETTI et al., 1994; PFISTER, 1999). In addition to hand-drawn precipitation maps, we consulted wind measurements (e.g., the Beckley anemometer from the summit of Säntis, at 2502 m a.s.l., for the 1890 event) or upper air information from tethered balloon and kite soundings at Friedrichshafen (Lake Constance) for the 1910 event (e.g., COAZ, 1869; BILLWILLER, 1876; ASMA, 1890, 1910, 1951).

3 Methods

3.1 Selection and analysis of meteorological fields

The amplitude of heavy precipitation events depends on the rate and duration of precipitation (DOSWELL et al., 1996). The rainfall rate is proportional to the vertical moisture flux, which is defined as the vertical wind times the mixing ratio of the rising air. The 20CR data provide information on quasi-geostrophically forced upward motion (approximated by the vertical motion at the 500 hPa level) and the vertically integrated moisture content of the atmosphere (i.e., precipitable water). The equivalent potential temperature (Θ_e) at 850 hPa serves as an air mass marker, and the wind field at 850 hPa represents low-level air flow.

Due to the resolution of 20CR, we can readily visualize and describe the large-scale patterns (cf. RUDARI et al., 2005). However, meso-beta-scale (and smaller) components must be deduced from other sources (see the Supplement available online). Local observations (e.g., wind drift, persistence of rainfall) and assessments by contemporary experts (e.g., Billwiller, Coaz) complete the descriptions.

3.2 Event selection

We define extreme floods as maxima in the time series of annual floods and lake levels (HQa). Except for Lake Constance, the series are influenced by human activities such as river regulations (e.g., WETTER et al., 2011). To account for this artificial signal, we quantify the difference between observed annual floods (or lake levels) and a mean contemporary annual flood (or mean lake level). A contemporary annual flood is defined as the 11-year moving average of the HQa. To define extreme floods, we use the 95th percentile of these differences over the entire record. Documentary evidence (see STUCKI and LUTERBACHER, 2010) enables us to include the Lago Maggiore event in 1868. This reveals the 24 flood events listed in Fig. 2 (hereafter referred to as "extreme floods"). We analyze the meteorological situation of these events using 20CR and ASMA.

We select particularly extreme floods to be explored in greater detail (e.g., the hydro-climatologic history). These floods correspond to the 98th percentile and consist of 12 events (1868, 1876, 1881, 1890, 1907, 1953, 1987, 1993, 1999 (two events), 2000, and 2005). We substitute the event of 1881 with the extreme event of 1910, because the latter was among the most spatially extensive floods in Switzerland, is better documented, and shows similar meteorological patterns to 1881. We include the Christmas flood of 1882 because all other events occurred during the warm seasons (May to October).

These 13 events are hereafter referred to as "the subset." They affect different regions (e.g., only the northern or southern side of the Alps), and are well-documented in the literature (e.g., RÖTHLISBERGER, 1991; AMBROSETTI et al., 1994; PFISTER, 1998; PFISTER, 1999; SCHMOCKER-FACKEL and NAEF, 2010; STUCKI and LUTERBACHER, 2010) and in the EuroClimHist database (EuroClimHist, 2008). Results for the subset are summarized in Table 1 (see Section 5). The meteorological analysis of the subset enables the meteorological classification of all 24 extreme floods (see Section 5). In the following section, we present examples for the subset events prior to 1950. More recent events are excluded because they are already comprehensively discussed in the literature (see Section 1).

4 Case studies of extreme floods since 1868

4.1 Lago Maggiore and Valais, September/October of 1868

The flood in the autumn of 1868 occurred in two episodes within a week. The first episode started on September 27th and affected southern, south-central and south-eastern parts of the Swiss Alps (Ticino, Graubünden, and St. Gallen; ARPAGAUS, 1870). The second episode began on October 3rd and affected the southern, central and western Swiss Alps (Ticino, Valais, and Uri; PETRASCHECK, 1989). The corresponding areas are presented in Table 1. Fifty casualties were registered in Switzerland. Approximately half of the financial losses were incurred in the Ticino (PFISTER, 1999). The level of Lago Maggiore (199.98 m a.s.l. on October 4th, 1868; FOEN) exceeded all (known) high water marks since 1177 (PFISTER and SUMMERMATTER, 2004). It was 0.9 m higher than the second largest flood since 1177 (in 1807; STUCKI and LUTERBACHER, 2010; based on AMBROSETTI et al., 1994, among others), and it was 2.6 m higher than the largest flood since 1868 (in 2000; Fig. 2).

4.1.1 Hydro-climatological disposition

Several wet spells on the AS, during the summer of 1868, brought precipitation sums of 40–50 mm/day and monthly precipitation sums above the 1961–1990 climatological mean (see the Fig. 2a Supplement, see ASMA, 1868; see the summary in Table 1). Precipitation in September was excessive (i.e., up to three times the reference monthly mean at Lugano). Consequently, the lake level at Locarno rose 6 m between September 20th and October 4th, 1868 (see the Fig. 2c Supplement).

4.1.2 Precipitation patterns

For this event, the highest amounts of precipitation were recorded at the San Bernardino Ospizio station (located at the San Bernardino Pass, 2065 m a.s.l.). Over the eight days (September 27th to October 4th), 1118.2 mm of rainfall was measured (cf. RÖTHLISBERGER, 1991; Fig. 3f and Table 1 for 24 h and 72 h amounts).

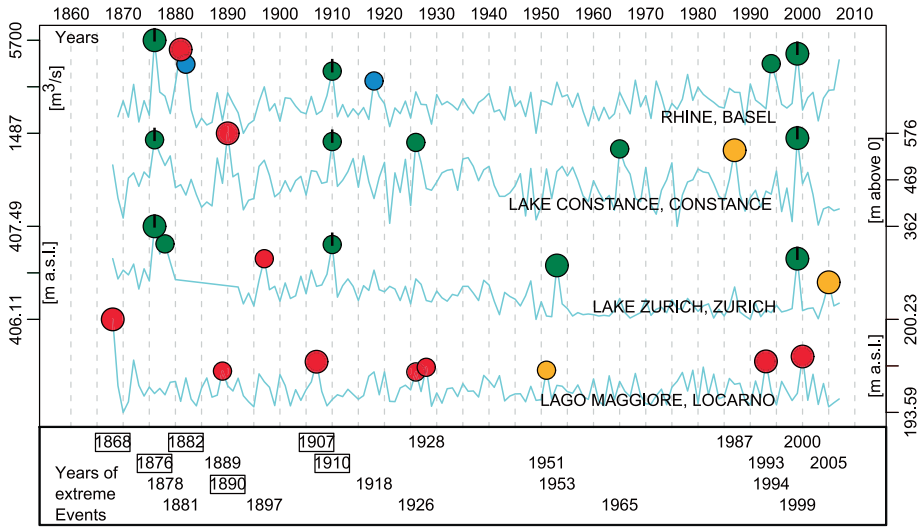

Figure 2: Time series of annual floods (HQa; light blue lines) for selected stations since 1868. Smaller circles indicate extreme floods (95th percentile), larger circles show the most extreme floods (98th percentile; with 1868 and 2005 introduced manually). Black tips indicate floods occurring in several catchments. Colors indicate the time of year. Eight events occurred in May and June (green), three occurred in August (yellow), ten took place in September, October, November (red), and two occurred in December (blue). Below, we provide the 24 extreme events (two events in 1926 and 1999, respectively). The framed years indicate events discussed in this study (the events in 1868, 1876, 1882, 1890, 1907, and 1910).

As shown in Fig. 3f, there was considerable spatial heterogeneity in the amounts of precipitation (cf. Section 5.2). During the second episode, precipitation fell over a larger area to the southwest and the overall amount was reduced (e.g., 196 mm was measured at the San Bernardino Pass on October 1st).

In addition, the weather reports from COAZ (1869) indicate fresh snow on higher elevations on September 23rd (e.g., 14 cm on the Julier Pass, 2284 m a.s.l.) and September 28th (visual observation on Rheinwaldhorn). Snow melt is attributed to high temperature, which were especially dramatic on September 27th and October 3rd (e.g., Splügen at 1460 m a.s.l., 16 °C and 18 °C; PETRASCHECK, 1989; cf. temperature at Lugano is provided in the Fig. 2b Supplement). The thaw was accompanied by heavy rainfall, hail, and thunder. These elements (i.e., sharp temperature rise, heavy precipitation, and snow melt) are listed as flood triggers in Table 1.

4.1.3 Atmospheric conditions

The first episode of precipitation started on September 28th. Between a mid-tropospheric cut-off low over the Celtic Sea and a ridge over southeastern Europe (Fig. 3a), a southwesterly flow was established over central Europe. Wind direction and cloud-drift observations at San Bernardino (south/south; ASMA, 1868) and at the Gotthard Pass (southeast/south) indicate a southerly flow over the Alps on September 28th, which is consistent with the wind field at 850 hPa in the 20CR data set (not shown).

The second episode of precipitation started on October 1st when an elongated upper-level trough over the Bay of Biscay moved southward with lifting along its eastern flank (Fig. 3b and c). At the surface, a secondary low pressure center formed over the western Mediterranean (i.e., Balearic Islands). The trough over the Bay of Biscay and the anticyclone over the Ionian Sea remained approximately stationary until October 4th (not shown), enabling a continuous flow of moist air from the central Mediterranean towards the Alps. Fig. 3d shows a clear counterclockwise turn of low level winds towards a southeasterly flow over northern Italy on October 2nd. Accordingly, winds were predominantly southeasterly at the Alpine passes (i.e., Gotthard, Simplon, and Grand St. Bernard) and at the AS stations (Lugano and Bellinzona; ASMA, 1868). This shift of wind direction is consistent with the westward drift of heavy precipitation (e.g., peak of daily precipitation at the Grand St. Bernard Pass was 78 mm on October 1st and at the Grimsel Pass was 59 mm on October 3rd, respectively; ASMA, 1868; see the Fig. 2d Supplement).

The southerly flow of warm and moist air in the lower troposphere (Fig. 3d) was maintained by the slightly eastward propagation of the Balearic cyclone on October 3rd and the stationary Ionian anticyclone (Fig. 3e). The October 3rd air temperature at Splügen (18 °C; 1475 m a.s.l.) indicates the local 850 hPa temperature and dew point in near-saturated air due to prevailing heavy precipitation, thunderstorms, and hail. Dew point temperature was probably in the range of 15 to 18 °C. Ascending air under these moist adiabatic conditions reaches freezing level at 4000 to 4500 m a.s.l., which leads to considerable snow melt and runoff at lower elevations.

The 20CR ensemble mean clearly indicates the two pulses of large-scale moisture transport towards the AS. Due to the convex Alpine model orography, the

Table 1: A hydro-climatological overview of 13 extreme floods in Switzerland since 1868. Columns Flood: The spatial extent of damage area (the black areas of the hexagon; cf. Fig. 1), gauge stations with extreme discharge or runoff (MAG: Lago Maggiore, BSL: Rhine Basel, CON: Lake Constance, and ZRH: Lake Zurich), the day of year with the greatest mean daily discharge/lake level (MQd)/annual flood (HQa), and the event's ranking in the HQa time series. Columns Hydro-climatology: Hydro-climatological disposition and trigger elements. These are: cold (CC) and warm (WW) periods, fast temperature rise (CW), period with heavy precipitation (RR), enhanced snow accumulation or snow pack (SS), intensive snow melt (MM), saturated soils (ST), and high lake levels (or runoff; LL). Lowercase letters indicate seasons. Associated visual symbols are added. Columns Precipitation: The spatial extent of heavy precipitation (HP; the black areas of the hexagon), date, precipitation sums (totals), and the station name with a daily (24 h) or three day (72 h) record of precipitation.

		Flood				Hydro-climatology		Precipitation						
		Region and time series ranking				Long- and short-term elements			Records 72 h			Records 24 h		
Year	Class	Damage area	Basin	Record date	Rank / Total	Disposition	Trigger	Extent Core HP Area	Date	Sum [mm]	Station	Date	Sum [mm]	Station
1868		SW-S	MAG	10-4	1/140	CCsp WWsu RRsu RRau	CW RR MM	SW-S	Sep 26 – 28	540.5	Bernardino Pass	Sep 28	254	Bernardino Pass
1876		N-NE	BSL ZRH CON	6-13 n.a. 6-18	1/139 4/186 5/191	SSwi CCsp SSsp RRsp STsp	CW RR	N-NE	Jun 11 – 13	316.4	St. Gallen	Jun 11	220	St. Gallen
1882		NW-N-NE	BSL	12-28	6/139	CCau RRau LLau	CW RR MM	NW-N-NE	Dec 25 – 27	194.1	Ebnat-Kappel	Dec 27	71	Ebnat-Kappel
1890		S-SE	CON	9-3	3/191	CCwi CCsp CCsu RRsu	WW RR	S-SE	Aug 27 -29	323.0	Locarno-Muralto	Aug 29	175	Bad Ragaz
1907		S	MAG	10-18	5/140	SSwi CCsp CCsu RRau	WW RR	S-N	Oct 14 – 16	421.4	Mosogno	Oct 16	199	Mosogno
1910		N-NE	BSL CON ZRH	6-16 6-28 6-17	7/139 6/191 14/186	SSwi CCsp RRsp STsp LLsp	WW RR MM	N-NE	Jun 13 -15	279.1	Rigi-Kulm	Jun 14	198 215	Rigi-Kulm Bödele
1953		N-NE	ZRH	6-28/29	42/186	WWsp RRsp	CW RR	N-NE	Jun 24 – 26	258.7	Weesen	Jun 26	121	Weesen
1987		SW	CON	(7-29)	(13/191)	SSwi CCsp RRsp RRsu WWsu LLsu	WW RR MM	S-N	Aug 23 – 25	356.4	Cevio	Aug 24	236	Cevio
1993		SW-S	MAG	10-9	4/140	RRsu STau	WW RR	SW-S	Sep 22 – 24	372.8	Cevio	Sep 24	146	Cevio
1999a		NW-N-NE	BSL	5-13 5-12	3/139	SSwi MMwi SSsp RRsp STsp LLsp	WW RR MM	NW-N-NE	May 11 – 13	191.1	Küsnacht (ZH)	May 12	100	Appenzell
1999b		N-NE	CON	5-24	4/191			N-NE	May 20 – 22	187.7	Säntis	May 21	139	Hohen-peissenberg
2000		SW-S	MAG	10-17 10-16	2/140	SSau RRau STau LLau	CW RR MM	SW-S	Oct 13 -15	310.2	Saas Fee	Oct 14	141	Saas Fee
2005		N-NE	BSL	8-23	22/139	RRsu STsu LLsu	CW RR MM	N-NE	Aug 20 – 22	221.6	Entlebuch	Aug 22	187	Säntis

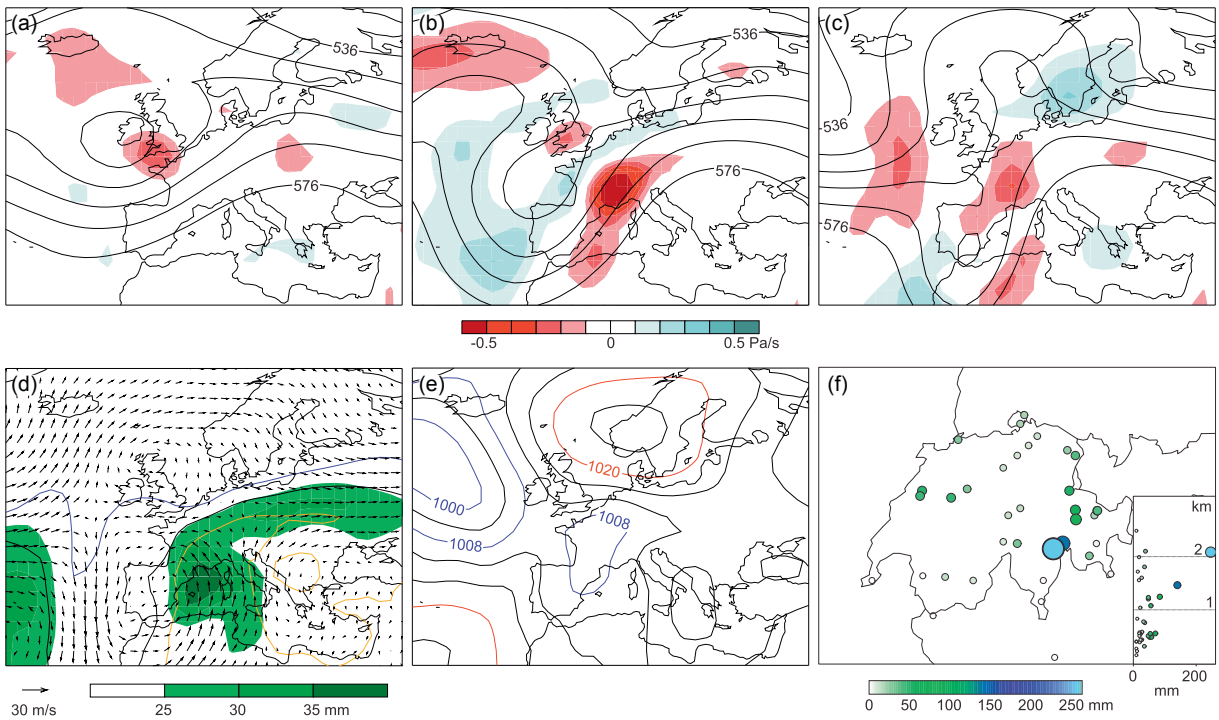

Figure 3: (a-c): 20CR geopotential height (in decameters; as solid black lines) and vertical motion (ascent indicated with red shades, descent indicated with steel-blue shades) at 500 hPa: (a) on September 28th, 1868 (at 12 UTC), (b) on October 1st, 1868 (at 12 UTC), and (c) on October 3rd, 1868 (at 12 UTC). (d): Θ_e (where blue, black, and yellow isolines show 16, 24, and 32 °C) and wind (as black arrows) at 850 hPa, and precipitable water (green shading) on October 2nd, 1868 (at 12 UTC) as calculated from 20CR. (e): Sea level pressure (hPa provided with red, black, blue lines) on October 3rd, 1868 (at 12 UTC) as calculated from 20CR. (f): Observed daily precipitation amounts at Swiss (and Swiss-bordering) stations from MeteoSwiss, DigiHom (FÜLLEMANN et al., 2011), and ECAD (KLEIN TANK et al., 2002) on September 28th, 1868. Data from COAZ (1869) are added in (f). The station with the maximum daily record (see also Table 1) is marked with a bold black ring. Station elevation versus precipitation rate is shown in the inset.

reanalysis possibly simulates airflow deflection at lower levels rather than convergence during the first episode. However, it captures the counterclockwise rotation of the flow during the second episode.

To conclude, the key conditioning factors for the flood were above-normal amounts of precipitation in the months preceding the event, intense precipitation in the days leading to the event, and considerable snow melt associated with a sharp temperature rise. The large-scale weather patterns indicate a slow progression of an upper-level trough over western Europe, associated mid-tropospheric lift, and a leftward turn of southerly winds at lower levels over northern Italy during the second episode. Modern analogues are presented in Section 5.2 and Fig. 9.

4.2 Basel, June of 1876

The Rhine River in Basel reached a maximum discharge of 5700 m^3/s during the event from June 10th to 13th. This is unprecedented for the instrumental period (WETTER et al., 2011; see the Fig. 2 and 3 Supplement). In addition, areas of the Swiss Plateau, Uri, and Graubünden were flooded (PFISTER, 1999; see Table 1 for selected flood levels). The total loss amounted to 14 million francs (CHF) value at that time (PETRASCHECK, 1989; in RÖTHLISBERGER, 1991).

4.2.1 Hydro-climatological disposition

BILLWILLER (1876) attributed the flooding to the melting of "tremendous amounts of yet accumulated snow masses in the mountains". In February and March of 1876, heavy precipitation fell on the Swiss Plateau (e.g., up to three times the 1961–1990 monthly means at Zurich; BEGERT et al., 2007; see the Fig. 3c Supplement). The remainder of spring was cold and wet. In Bern, for instance, mean daily temperature in May was approximately 5 °C below the 1961–1990 monthly mean. In early June, daily mean temperatures rose, eventually exceeding one standard deviation relative to the 1961–1990 reference period (compare with the Fig. 3a and b Supplement). According to RÖTHLISBERGER, 1991 (Table 1), the floods were triggered by "long lasting excessive rainfall and intense thunderstorms on saturated soils" along the AN.

4.2.2 Precipitation patterns

Considerable amounts of precipitation were measured on both sides of the Alps at an early stage of the event (e.g., 76 mm at Bad Ragaz on the AN on June 7th, and 101 mm at Lugano on the AS on June 10th; see the Fig. 3d Supplement). From June 10th to June 13th, precipitation

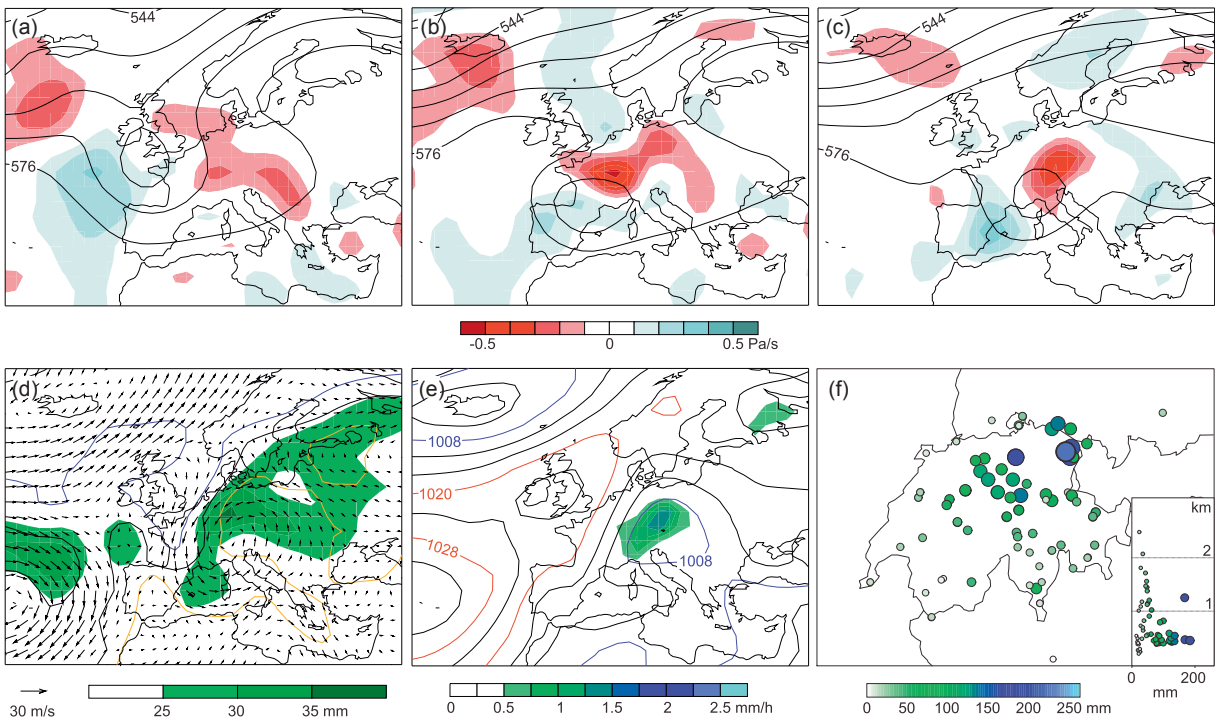

Figure 4: As in Fig. 3. (a-c): June 9th (at 12 UTC) to June 11th (at 12 UTC), 1876. (d): June 11th, 1876 (at 12 UTC). (e): June 11th, 1876 (at 12 UTC). In (e), green shading shows the hourly precipitation rate over 3 hours. (f): June 11th, 1876. Data from BILLWILLER (1876) are added in (f).

on the AN was nearly continuous, peaking on June 11th–12th. Between June 11th and June 13th, 316.4 mm accumulated at the St. Gallen station (Table 1). All June 11th precipitation measurements mentioned in BILLWILLER (1876) are included in Fig. 4f. On this day, thunderstorms were reported in Zurich, and thunderstorms and hail were observed in St. Gallen.

4.2.3 Atmospheric conditions

On June 9th, the upper-level flow over Europe was characterized by two prominent synoptic-scale features, a strong ridge over Russia and a cut-off low/trough over the British Isles (Fig. 4a). Over the next two days, the cut-off low moved northeastwards from the Pyrenees and crossed the Alps (Fig. 4b and c).

At low levels, a distinct cold front established over northwestern Europe and moved southward towards the Alps until June 11th (cf. Fig. 4d). A persistent northeasterly low-level flow prevailed along the Alpine north side (Fig. 4e).

The upper-level cut-off low and the associated warm air advection to the east (Fig. 4d) led to conditionally neutral to unstable atmospheric stratification (not shown). These conditions favored stratiform precipitation and embedded thunderstorms, as suggested by the observed precipitation patterns (Fig. 4f). Stratiform precipitation led to elevation-independent amounts of precipitation, whereas spatially variable amounts of precipitation on the Swiss Plateau are typical for convective precipitation.

The model-generated 20CR precipitation field (Fig. 4e) is associated with a zone of moisture flux convergence at 850 hPa (not shown) impinging on the AN from the northeast. A time series of daily precipitation for a grid-point over the Alps (46.7 °N, 9.4 °E) reveals that the event is captured. However, the grid cell precipitation signal in the 20CR ensemble mean is low compared to the observed local maxima (e.g., 20 mm/day compared to 220 mm/day recorded at the St. Gallen station on June 11th; see Fig. 4f ; see Table 1; see the Fig. 2c to d Supplement). In addition, several precipitation events of comparable amplitude occurred between February and June of 1876 in the 20CR data set. However, the observations suggest that the June event was at least twice as intense as any other precipitation events in the spring of 1876 (see the Fig. 3d Supplement).

To conclude, the 1876 event was mainly preconditioned by a wet spring and the presence of considerable snow cover. The precipitation that triggered the event resulted from a steady northeasterly low-level flow of moist air towards the AN and the slow progression of the weather system to the east, and it was favored by large-scale lifting associated with the upper-level cut-off low.

4.3 Rhine/Basel, December of 1882

In 1882, an early winter flood lasted from December 25th to 27th. The return period of the discharge at Basel was comparable to the 1817, 1994, and 2007 events (WETTER et al., 2011). The mean daily discharge (MQd) at Basel

Rheinhalle was 4371 m^3/s, which is the 5th highest value in the station history (Fig. 2). Damages from the flood were reported from western to northern parts of Switzerland (RÖTHLISBERGER, 1991).

4.3.1 Hydro-climatological disposition

Autumn of 1882 was wet on the AN (i.e., snow sums in November reached the 95th percentile of the 1901–1950 period; e.g., Elm at 960 m a.s.l.; cf. STUCKI and LUTERBACHER, 2010). However, December was fairly dry until Christmas (cf. the Fig. 4c Supplement). From November to December, temperatures were below the 1961–1990 average, with occasional warmer spells. However, temperature increased rapidly between December 25th and 27th (e.g., from -12 °C to 2 °C at the Grand St. Bernard Pass; 2470 m a.s.l.; ASMA, 1882; see the Fig. 3a to b Supplement). RÖTHLISBERGER (1991) reported "sudden snowmelt and extraordinary rainfall" as triggering factors for the flood (Table 1).

4.3.2 Precipitation patterns

On December 23rd, heavy precipitation and snowfall were observed on the AN. For instance, measurements from Elm (960 m a.s.l.) indicate a 38 cm snow layer with a water equivalent of 32 mm (see the Fig. 4d Supplement).

Between December 25th and 27th, cumulative precipitation approached 200 mm in the eastern AN (194.1 mm at Ebnat-Kappel; see Fig. 5f; see Table 1). Precipitation fell on the Jura, the Swiss Plateau, and the pre-Alps. However, the AS and inner-alpine valleys remained dry. At stations above 700 to 800 m a.s.l., snowfall was reported from December 21st to 25th, and a mixture of snow and rain fell on December 26th and 27th (ASMA, 1882). On December 24th, it snowed in Geneva, Neuchatel, Bern, and Zurich. Basel experienced snow and rain (ASMA, 1882).

4.3.3 Atmospheric conditions

On December 25th, an intense extra-tropical cyclone was located in the mid-Atlantic (Fig. 5a). On December 27th, a second cyclone reached the eastern Atlantic (Fig. 5e), exhibiting the typical T-bone structure of the Shapiro-Keyser model (SHAPIRO and KEYSER, 1990). This was reflected in the distinct pattern of mid-tropospheric ascent (Fig. 5c) and in the precipitation rate. In the warm sector of the cyclone, mild (up to 10 °C at 850 hPa) and moist air was advected towards the Alps (Fig. 5d). Accordingly, the Säntis summit station reported a wind shift from north to southwest between December 25th and 27th (ASMA, 1882). Over several days, recurring advection of moisture towards the Alps by strong winds led to prolonged precipitation. This was especially apparent in the eastern areas of Switzerland (see the Fig. 5f and the Fig. 4d Supplement).

20CR reproduces the repetitive passage of frontal systems associated with three pulses of precipitation (on December 25th, 26th, and 27th). Precipitation magnitudes are underestimated by a factor two to seven (a maximum of 25 mm/day) compared to local observations. This is ascribed to the location of the precipitation field cores to the north of the Alps in the ensemble mean (see Fig. 5f; see Table 1; see the Fig. 4d Supplement).

In summary, a northwesterly flow produced prodigious snow on December 23rd and 24th at lower elevations. Moist and mild mid-Atlantic air was advected repeatedly to northern Switzerland (see Fig. 9 for a generalized schematic). A temperature increase, large amounts of precipitation, and strong winds led to a rapid melting of the snow pack on the Jura Mountains, the Swiss Plateau, and the Alps.

4.4 Lake Constance, August of 1890

In August of 1890, severe floods and landslides occurred in eastern Switzerland and the Ticino. Losses of CHF 850'000 were reported in 134 municipalities in the Canton of Graubünden. Rhine dams broke in Vorarlberg, flooding the Alpine Rhine valley. On September 3rd and 4th, the third highest annual flood levels since 1817 were recorded in Constance (2.35 m above the mean level of 1902–2006; LUBW; cf. Fig. 2 and Table 1). Billwiller (in ASMA, 1890; see the Fig. 5c Supplement) reported a 1.5 m rise of Lake Constance from August 24th to September 2nd and a 2 m transgression of Lake Walensee from August 28th to 31st.

4.4.1 Hydro-climatological disposition

Measurements at Bad Ragaz (500 m a.s.l.) indicate a cold to very cold period from the end of May to early August, followed by a rapid rise in temperatures (see the Fig. 5a Supplement). Precipitation at Bad Ragaz was generally within quartiles of the 1961–1990 period until May (cf. the Fig. 5c Supplement). In June and July, the monthly sums (approximately 290 mm each) were equivalent to 2.5 times the reference period average. The monthly sums in August reached 769 mm (ASMA, 1890).

4.4.2 Precipitation patterns

On August 24th, there was heavy precipitation in the Ticino and the Rhine valley (120 mm at Bad Ragaz; see the Fig. 5d Supplement). Continuous rainfall followed until August 25th (BILLWILLER and BÜHLER, 1891; RÖTHLISBERGER, 1991; EuroClimHist, 2008). During a second, more intense episode of precipitation (from August 27th), considerable amounts of precipitation

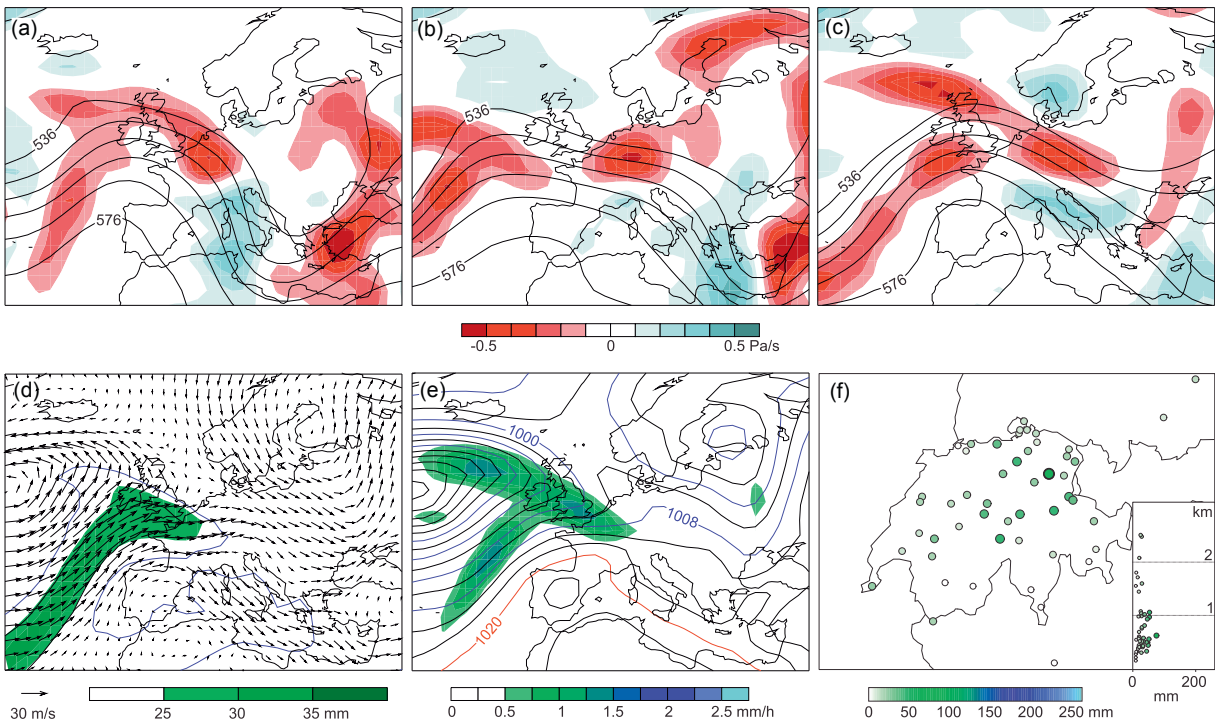

Figure 5: As in Fig. 4. (a-c): December 25th (at 12 UTC) to December 27th (at 12 UTC), 1882. (d-e): December 27th, 1882 (at 06 UTC). (f): December 27th, 1882.

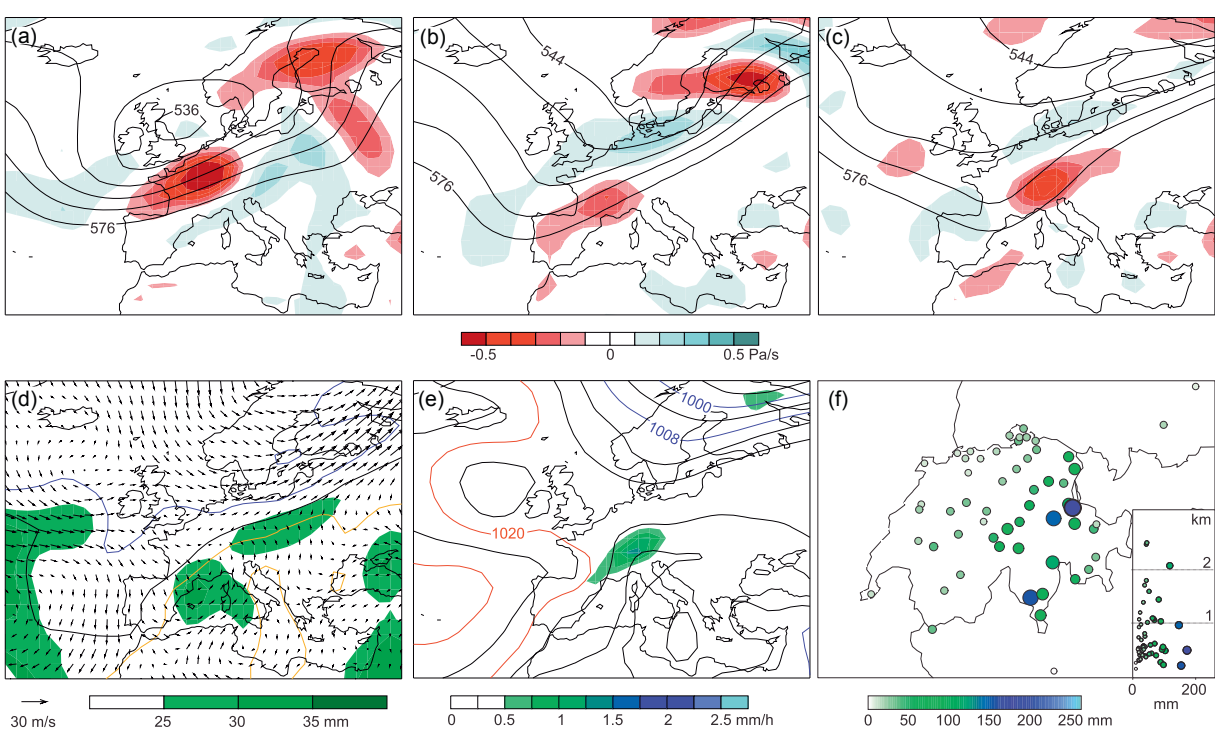

Figure 6: As in Fig. 4. (a-c): August 27th (at 12 UTC) to August 29th (at 12 UTC), 1890. (d): August 29th, 1890 (at 06 UTC). (e): August 29th, 1890 (at 12 UTC). (f): August 29th, 1890.

fell in the Ticino (98 mm at Locarno; see the Fig. 5d Supplement) and in northeastern Switzerland (Fig. 6f). On August 29th, the precipitation at Bad Ragaz (175 mm) was a maximum for the station history. Between August 27th and 29th, the 72 h precipitation observed at Lugano was 323 mm (see Table 1). The magnitude of heavy precipitation appeared to be independent of station elevation (Fig. 6f).

4.4.3 Atmospheric conditions

Between August 24th and 26th, an upper-level trough and an associated low pressure system moved over Central Europe (not shown). By August 27th, a second low was established over the British Isles. As this low slowly moved eastward (Fig. 6a), it was accompanied by a large-scale diurnal cycle of convection, which is reflected in ascending air at the 500 hPa level (Fig. 6a to c), and strong low-level convergence. Temperature differences of $\geq$18 °C across the 700 hPa–500 hPa layer (not shown) indicate static instability over the Mediterranean region.

On August 28th, the eastern part of the upper-level trough reached the Alps and the system became quasi-stationary (Fig. 6b and c). The following day, the associated cold front reached the Alps (Fig. 6d). Accordingly, mid-day temperatures at Altstätten decreased from 24.3 °C (on August 27th) to 10.9 °C (on August 31st; see the Fig. 5b Supplement for Bad Ragaz). On August 28th, high Θ_e air of the cyclone's warm sector was driven towards the Alps by southwesterly winds. The formation of a weak low pressure system over the Gulf of Genoa caused low-level winds to turn from southwest to south. The surface low migrated eastward. When it reached northern Italy (i.e., the Adriatic Sea), precipitation set in at the eastern AN (Fig. 6e). Fig. 6f shows a heterogenous spatial distribution of precipitation. This indicates deep convection drifting into the northern foreland of the Alps, which is consistent with reports of heavy rain, thunder, and hail (ASMA, 1890).

The 20CR ensemble mean suggests approximately 20 mm/day of precipitation over the Alps. This is substantially less than the observed precipitation (see the Fig. 6f and Fig. 5b Supplement). However, the progression and timing of the precipitation field agrees with the maximum observed precipitation (see the Fig. 5c to d Supplement; see Table 1).

In summary, the summer of 1890 was very wet and cold. The synoptic-scale setting during the intense precipitation at the end of August was characterized by repetitive mid-tropospheric ascent and stationarity of the second frontal system. Moist and warm air was advected towards the AS along a southwest-northeast oriented surface cold front. A generalization of the large-scale patterns is given in Fig. 9.

4.5 Lago Maggiore, October of 1907

On October 18th, 1907, several lakeside towns on Lago Maggiore were flooded (Autorità di bacino del fiume Po; www.adbpo.it; accessed online in March of 2011) and the market place in Locarno was submerged (ASMA, 1907). The water level of Lago Maggiore was 4 m above average (197.1 m a.s.l.). This is approximately 3 m below the 1868 level, but equivalent to the 1993 flood (Fig. 2).

4.5.1 Hydro-climatological disposition

On the AS, spring and summer temperatures were below the 1961–1990 mean. In August and September, temperature exceeded the monthly average (see the Fig. 5a and b Supplement for temperature at Lugano; cf. also Table 1). From January until the end of August, precipitation in Lugano was below the 1961–1990 monthly means (BEGERT et al., 2007). However, rainfall in September was approximately double and in October was almost triple the monthly average (e.g., 1128 mm at Borgnone/Centovalli in October; Billwiller in ASMA, 1907). These wet conditions lasted 37 days (i.e., September 25th to October 31st, 1907; see hydro-climatological elements in Table 1; see the Fig. 6c Supplement).

4.5.2 Precipitation patterns

Heavy precipitation occurred in two episodes (ASMA, 1907). During the first episode (from October 8th to and 9th), most precipitation was focused along the western Jura and the western Ticino. This led to a 1.3 m transgression of Lago Maggiore (see the Fig. 6c and d Supplement). The second episode began on October 14th, with daily precipitation sums of 100 mm in the Lago Maggiore area. On October 15th, 100 mm of precipitation was measured in eastern Valais and at the Gotthard Pass. However, a maximum occurred in the Ticino (142 mm at Mosogno; see the Fig. 6d Supplement). On the following day, the same station received 198 mm (Fig. 7f). Over 72 h (October 14th to 16th), the station had a total amount of 421.4 mm (Table 1). Thunderstorms with intense lightning activity were observed in Graubünden and the Ticino on October 15th and 16th (ASMA, 1907).

4.5.3 Atmospheric conditions

From October 14th to 16th, a deepening trough over the eastern Atlantic and the Bay of Biscay dominated the synoptic-scale flow over Europe (Fig. 7a to c). Strong ascent occurred along the eastern flank of the trough. Persistent winds in a northward flow of Saharan air over the warm Mediterranean transported unusually large amounts of precipitable water (i.e., unusual for mid-October; 25–30 mm; Fig. 7d). On October 16th, a secondary low pressure zone was established over the north-western Mediterranean (i.e., the Gulf of Lions), which contributed to the southerly warm moisture flux over northern Italy (Fig. 7d to e). On October 16th, the winds at Lugano (AS) and Säntis (AN) turned to the east (ASMA, 1907). Accordingly, the precipitation field shifted slightly to the west across the Alpine crest line (see the Fig. 7f and Fig. 6d Supplement).

A 20CR grid-cell representing the AS (44.8 °N, 9.4 °E) indicates that the maximum precipitation on

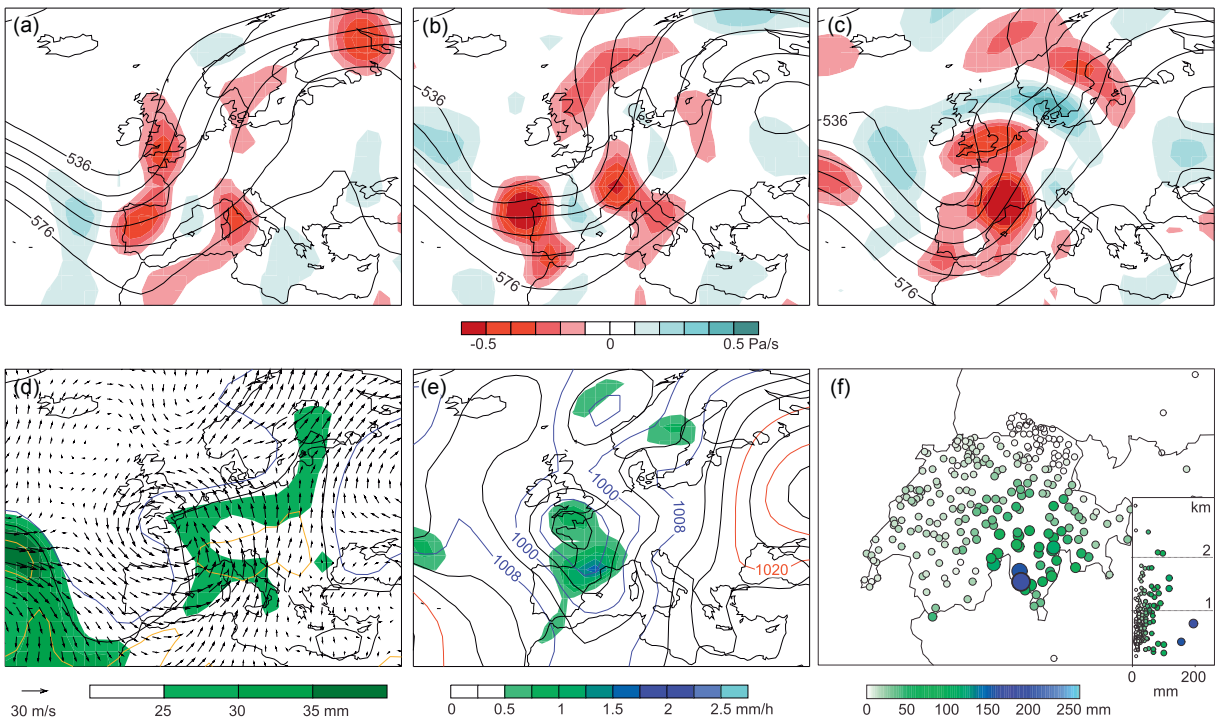

Figure 7: As in Fig. 4. (a-c): October 14th (at 12 UTC) to October 16th (at 12 UTC), 1907. (d): October 16th, 1907 (at 18 UTC). (e): October 16th, 1907 (at 12 UTC). (f): October 16th, 1907.

October 17th, 1907, was 30 mm (see the Fig. 6d Supplement). This is five times less than the amount reported for the previous day at Mosogno. Both reanalysis and observed values indicate the largest precipitation amounts in the respective time series covering four months. However, the 20CR ensemble mean mistakes the exact timing (6 to 12 hours late) and location of the heaviest rainfall (southern France; cf. see Fig. 7e).

In summary, the flood resulted from very wet and cold conditions in the preceding months. The extraordinary amount of precipitation was caused by strong synoptic ascent and a persistent southerly flow of moist air. Differences to the 1868 event are reviewed in Section 5.3 and Fig. 9.

4.6 Northern Switzerland, June of 1910

In June of 1910, heavy precipitation triggered one of the most spatially extensive floods in northern Switzerland (RÖTHLISBERGER, 1991). Record discharges were observed at the river stations Limmat (in Zurich), Linth (in Weesen), Rhine (in Reckingen), Rhine (in Basel; 4040 m^3/s on June 16th; cf. the Fig. 2 and Fig. 7c Supplement), and Thur (in Andelfingen). Transgressions occurred at lakes Thun, Brienz, Zurich (407.22 m a.s.l. on June 17th; Fig. 2), Lucerne, and Constance (ASCHWANDEN, 2000). In terms of record discharges, the June of 1910 flood is analogous to the 1999b flood (ASCHWANDEN, 2000). However, synoptic conditions are more similar to the 2005 flood (FREI, 2005; cf. Section 5). This event has been ascribed to heavy precipitation on saturated soils and extensive snow melt (RÖTHLISBERGER, 1991; included as determinative elements in Table 1).

4.6.1 Hydro-climatological disposition

In January of 1910, cold and wet conditions prevailed on the AN. By the end of the month, 40 cm of snow accumulated in Zurich (ASMA, 1910). Cold spells followed in spring, when temperature was near the freezing point in Zurich and was well below zero at Säntis (see the Fig. 7a Supplement). In May and June, monthly mean precipitation reached the 95th percentile of the 1961–1990 reference period. Early June was generally warm and sunny with scattered thunderstorms (ASMA, 1910; ASCHWANDEN, 2000). BILLWILLER (1910) emphasized that large positive temperature anomalies at higher elevations led to rapid snow melt, enhanced soil saturation, and greater discharges (see the Fig. 7a to b Supplement). Between June 1st and 10th, 132 cm of snow melted at Säntis, adding to enhanced river flow and soil saturation (cf. the Fig. 7c Supplement).

4.6.2 Precipitation patterns

Between June 9th and 12th, daily precipitation amounts of 50 mm were observed across the Swiss Plateau (cf. the Fig. 7d Supplement). On June 13th, the focus of precipitation shifted to the northeastern Alps. The highest values were observed on Rigi-Kulm at 1798 m a.s.l. (44 mm/

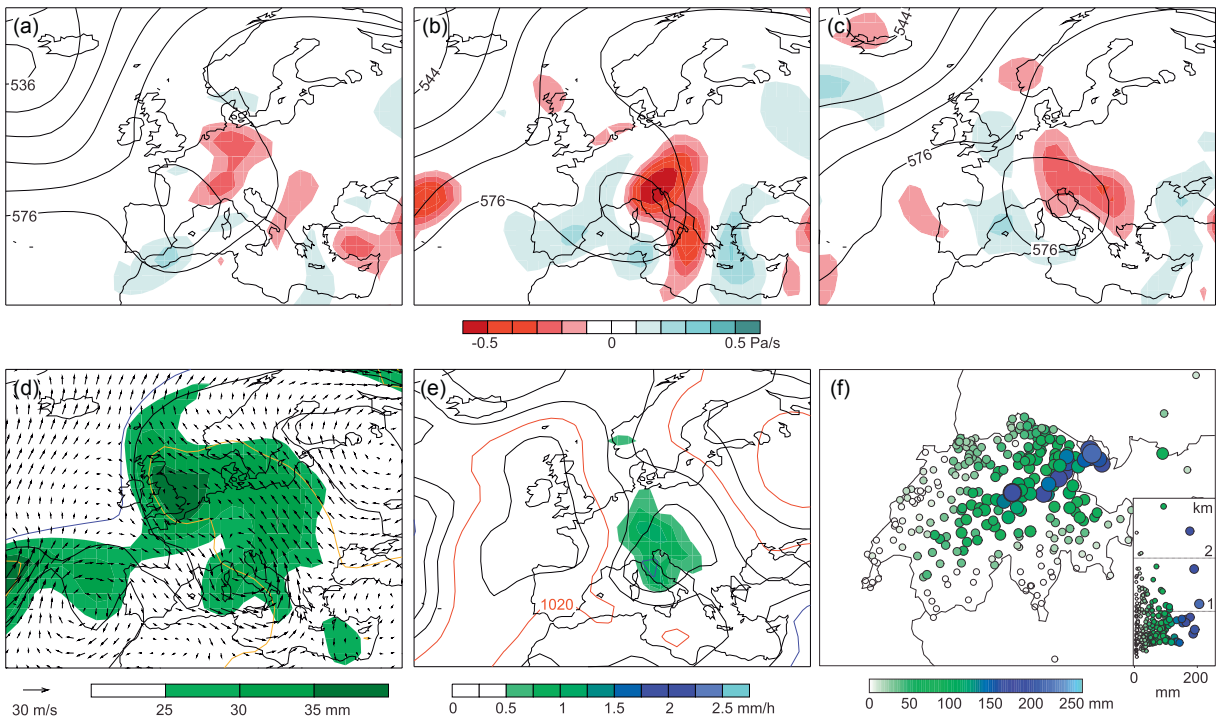

Figure 8: As in Fig. 4. (a-c): June 12th (at 12 UTC) to June 14th (at 12 UTC), 1910. (d): June 13th, 1910 (at 12 UTC). (e): June 14th, 1910 (at 12 UTC). (f): June 14th, 1910. Data from GODINA et al. (2006) are added in (f).

day; see the Fig. 7d Supplement). The eastern inner Alpine AN also experienced enhanced precipitation.

On June 14th, precipitation peaked. The heaviest rainfall occurred along the eastern pre-Alps (cf. FREI, 2005). On Rigi-Kulm, a daily sum of 198 mm and a 72 h sum of 279.1 mm (for June 13th to 15th, Table 1) were recorded. Extraordinary amounts of precipitation were observed at all elevations except for the lowest stations on the AS.

4.6.3 Atmospheric conditions

By June 12th, a mid-level cut-off low had moved from the Bay of Biscay to the western Mediterranean Sea (Fig. 8a). It intensified over the Ligurian Sea on June 13th and its axis turned to a south-east north-west orientation (Fig. 8b). Downstream, static stability was reduced over the eastern Alps (not shown) in an area of large mid-level ascent (Fig. 8b). A stationary ridge over Russia impeded the eastward progression of the cut-off low (Fig. 8c).

A surface low established over northern Italy on June 12th and remained quasi-stationary until June 15th (Fig. 8e). On June 13th, a moist and warm air mass was present over central and eastern Europe, while over western Europe, cold and dry air flowed towards the southeast (Fig. 8d). Winds at 850 hPa indicate a strong flow from east-southeast over the eastern Alps. Consistently, a tethered balloon sounding by the kite station at Friedrichshafen registered easterly winds between 1000 and 3500 m a.s.l. (ASMA, 1910).

This counter-flow (i.e., a clockwise turn of winds with altitude from north to east) intensified from June 13th to June 14th. The kite measurements at 6:30 AM on June 14th indicate northerly winds between 1000 and 3000 m.s.l. Observational data also show the presence of cold air in the valleys on the AN. Specifically, between June 12th and 14th, mid-day temperature at Altdorf (456 m a.s.l.) decreased by 5 °C (ASMA, 1910; cf. the Fig. 7b Supplement for Zurich and Säntis). Above 3000 m a.s.l., southeasterly winds persisted. This counter-flow situation induced ascending of the warm airstream over the lower cold air, which resulted in persistent, elevation-independent precipitation over the Alps (Fig. 8f; cf. BILLWILLER, 1910). Accordingly, sustained precipitation was reported in ASMA (1910). It intensified from extensive in the morning to "torrential" in the evening and during the night in central and eastern Switzerland.

The focuses of precipitation in the 20CR ensemble mean are co-located with areas of strong mid-level ascent. On June 13th, precipitation maxima in the reanalysis are on the AS and weaker precipitation occurs on the AN (cf. Fig. 8e). At the central Alpine model grid-point (46.7 °N, 9.4 °E), daily precipitation amounts hardly exceed 20 mm/day. These pale in comparison to the observed maximum of 200 mm/day at Rigi-Kulm (see the Fig. 6d Supplement). When considering precipitation at the same grid-point between February and July, the conditions on June 14th do not appear extraordinary.

To summarize, the hydro-climatological conditions were set by snow storage well into spring followed by very wet periods and large snowmelt leading to saturated soils (Table 1). The large-scale forcing (i.e., reduced static stability and enhanced ascent of warm and moist air) in a persistent counter-flow situation resulted in intense precipitation over the Alps. Refer to Section 5.1 and to Fig. 9 for comparisons to the 1876 flood or modern events.

4.7 Hydro-climatological overview

Table 1 provides a summary of the hydro-climatological situation for each subset event. This is based on the analysis of 20CR, station data, and documentary information. Five flood events occurred in catchments of the AS. Eight events primarily affected catchments of the AN (Table 1). By definition (see Section 3), most of the observed discharges rank among the top ten of the time series recordings.

With respect to the hydro-climatological setting, snow accumulation and snow storage (related to a cold spring and summer) are important variables (COAZ, 1869; BILLWILLER, 1876). Six events are strongly associated with this combination (1876, 1907, 1910, 1987, and 1999a and b). Extended periods (i.e., over several weeks) of heavy precipitation (and the resulting soil saturation, lake level transgressions, and enhanced fluvial discharges) are key prerequisites for all events. Note that soil saturation is only introduced in Table 1 if documentary information is available.

For eight events, heavy precipitation was accompanied by a rapid warming and melting of long- or short-term accumulated snow. Snowmelt may account for half of the runoff during an extreme flood (e.g., GREBNER and ROESCH, 1999; FORSTER and HEGG, 2000). Snowmelt was of minor importance for three flood events on the AS (1890, 1907, and 1993). However, high temperatures or a sharp temperature rise are a prerequisite for each subset event because the potential moisture content (and freezing level) of air is determined by temperature (e.g., RÖTHLISBERGER, 1994).

The daily and 72 hour precipitation of early events (i.e., before 1987) exceeded more recent events. The greatest 72 hour amounts were registered on the AS during the 1868 and 1907 autumn events. Daily precipitation in winter events is typically reduced, but in return the precipitation episode lasts longer.

5. Meteorological classification of the flood events

Based on the subset events, we derived a subjective meteorological classification of the flood-inducing weather situations. This involved an iterative process of visual pattern assessment, which started with the areas of heavy precipitation and flooding (Table 1). Then, we identified similarities in terms of: location, form, orientation, and propagation of various meteorological fields (i.e., upper-level geopotential height and regions of ascent, surface fronts, location of low and high pressure systems, and equivalent potential temperature and fields at 850 hPa).

The procedure was applied to all 24 extreme floods. We elected five atmospheric patterns (“types”) based on upper-level synoptic-scale flow, surface pressure features, temperature anomalies, and moisture transport. At the 500 hPa level, for instance, the types feature: (i) pivoting cut-off lows (filed isohypses), (ii) elongated cut-off lows, (iii) elongated troughs (high amplitude, small radius of isohypses curvature), (iv) waves (with a kink), and (v) zonal flow (approximately zonally-oriented parallel isolines). The five types are named after the most prominent atmospheric pattern and are shown in idealized form in Fig. 9.

5.1 Pivoting cut-off (PCO)

The conditions in June of 1876, June of 1910, May of 1999 (the 1999b event), and August of 2005, represent the pivoting cut-off (PCO). The upper-level flow of this type is characterized by a cut-off low over the Adriatic Sea with strong ascent along its north-eastern to northern sector. The term pivoting refers to the cyclonic path of the cut-off low around the Alps (i.e., from the north-western Mediterranean Sea/Gulf of Lions across northern Italy), and the shift of the main axis of symmetry from north-south to a more zonal orientation. The circulation associated with this vortex is evident in the 850 hPa level Θ_e and wind fields. They exhibit a characteristic S-shape, with enhanced easterly moisture transport in the northern lobe of the S-shape. Blocking surface highs, located over western and eastern Europe, lead to a near-stationarity of the system.

The PCO has two subtypes. During the 1910 and 2005 events, the cut-off low was approximately circular and the flow towards the Alps was from the north sector. Alternatively, the 1876 and the 1999b events had a zonally elongated cut-off low with advection from the northwest. Accordingly, the largest 72 h precipitation sums were measured in central (in 1910 and 2005) and northeastern (in 1876 and 1999) Switzerland, respectively (see Table 1; see FREI, 2005). Further PCO type events occurred in September of 1881, June of 1953, June of 1926, June of 1965, and May of 1994 (with partial or no blocking in the latter three; see also GREBNER and ROESCH, 1998). The SLP patterns of the PCO have similarities to the Vb track (van BEBBER, 1891) which are especially apparent in the initial phases. However, stationarity (and the further routes of the cut-off low towards the east or southeast) is determined by the exact location of the high over eastern Europe (cf. GREBNER and ROESCH, 1998; METEOSWISS, 2006).

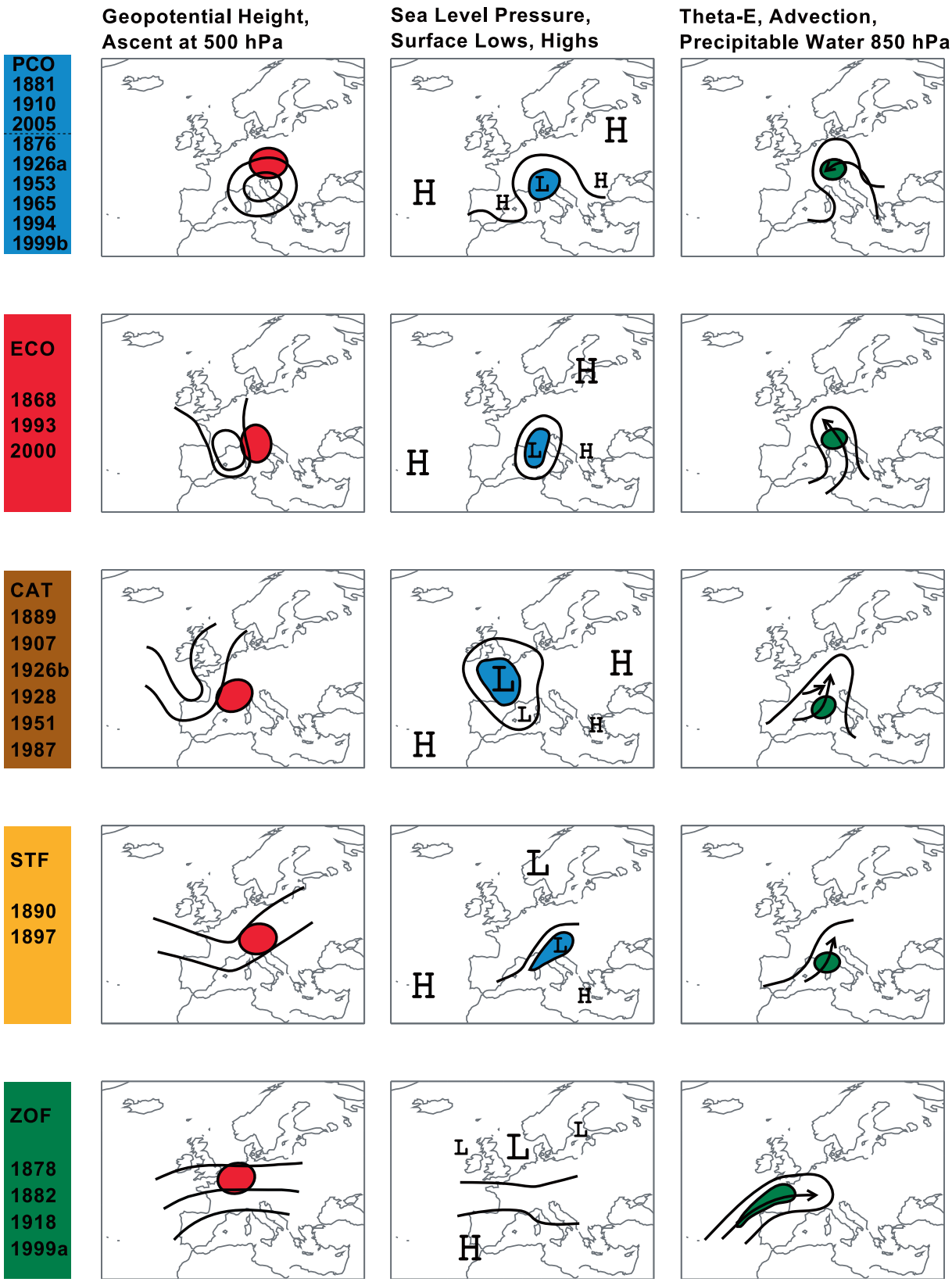

Figure 9: Schematic showing flood-causing atmospheric patterns categorized into five types (colored box with dates of representative flood events): PCO (Pivoting Cut-Off; subtypes separated by dashed line), ECO (Elongated Cut-Off), Canarian Trough (CAT), Stationary Front (STF), and Zonal Flow (ZOF). Left column: Geopotential height (as black lines) at 500 hPa and the core area of large-scale mid-tropospheric ascent (red field). Middle column: Sea level pressure (as black lines) and location of primary and secondary surface highs (H) and lows (L). Blue fields indicate stationarity. Right column: Areas of precipitable water (as green fields) with wind direction at 850 hPa (as black arrows) and the surrounding field of enhanced Θ_e (frontal structures; as black lines).

5.2 Elongated cut-off (ECO)

The October of 2000 and September of 1993 floods were similar to the event from September to October of 1868. The elongated cut-off (ECO) typically occurs in autumn and leads to extreme precipitation in southern/southwestern Switzerland. It is characterized by a meridionally-elongated trough at 500 hPa over the Balearic Sea and Gulf of Lions. From this trough, an elongated cut-off low develops and slowly progresses eastward. Ahead of it, large-scale lifting supports convection over the Alps and northern Italy.

The SLP field is dominated by a low pressure system over the northwestern Mediterranean Sea (see also MASSACAND et al., 1998; FREI et al., 2000; GREBNER et al., 2000; MASSACAND and WERNLI, 2001). The evolution is analog to findings by BUZZI and FOSCHINI (2000), who pointed to the dominance of convection and the counterclockwise rotation of the wind field which enhances southerly moisture advection.

5.3 Canarian Trough (CAT)

The floods in October of 1907 and (less clearly) August of 1987 belong to the CAT type, which shares similarities to ECO. However, the trough at 500 hPa evolves into a narrow and south-reaching form with its core located northwest of the Pyrenees. A strong surface low over Brittany is present. On the southern flank of this primary low, a secondary low forms over the Gulf of Lions and the Balearic Islands, which contributes to the warm moisture flux towards the southern Alps (cf. GREBNER and RICHTER, 1991; GREBNER and ROESCH, 1998; PFISTER, 1999). At 850 hPa, in contrast to the south-southeast flow of the ECO, the CAT has a south-southwest flow, but a weak counterclockwise change in flow direction is also present. Similar conditions occurred in October of 1889, November of 1926, October of 1928, and August of 1951, confirming that CAT is a typical autumn atmospheric pattern responsible for heavy precipitation reaching from the AS across the Alpine divide.

5.4 Stationary front (STF)

For the atmospheric conditions in August of 1890, we were unable to identify a modern equivalent. However, we did find similarities to the September of 1897 event. The trough at 500 hPa indicates enhanced updraft downstream of the curvature axis. This is the location of a quasi-stationary front (STF) along the Alps. There is a distinct zonally-elongated intrusion of low pressure along the AS at surface level. Accordingly, flow converges across the Alpine rim.

5.5 Zonal flow (ZOF)

The conditions in early June of 1878, December of 1882, December of 1918, and May of 1999 (the 1999a event), show how large amounts of precipitation can be produced in non-convective environments (cf. DOSWELL et al., 1996). Under ideal circumstances, the flow at upper-levels and at the surface shifts from northwesterly to near-zonal over the Alps and western Europe during the event. This sustains advection of moisture from the subtropical/mid-Atlantic area along a small band of enhanced Θ_e and precipitable water content (cf. LAVERS et al., 2011). 72 h precipitation sums approaching 200 mm can be observed in northeastern Switzerland (e.g., GREBNER and ROESCH, 1999; see Table 1). Rapid snow-melt (also at high elevations; related to large amounts of precipitation, increases in temperature, and strong winds) is an important contributor to the ZOF (e.g., METEOSWISS, 2006; for the mid-May of 1999 event).

5.6 Links to existing classifications

All 24 extreme floods listed in Fig. 2 could be assigned to one of the five types, and each type (except for STF) has both historic and recent examples.

We opted for a new classification system, which is independent to prior studies. This is because of differing study areas, missing information (e.g., WEHRY, 1967), and newly available datasets. Nevertheless, our types agree with (and complement) previous classification systems. For instance, STF class is similar to the quasi-stationary ("schleifende") front described by WEHRY (1967). The conditions assessed by HILKER et al. (2008), regarding the spatial distribution of the flooded areas and damages (in 1876, 1910, 1999, and 2005), are consistent with the PCO. A number of southern inflow weather situations associated with elongated cut-offs or troughs (MASSACAND et al., 1998; BUZZI and FOSCHINI, 2000; MARTIUS et al., 2006; among others) correspond to the ECO. Finally, ZOF is consistent with the atmospheric patterns of winter floods in Central Europe (STURM et al., 2001; JACOBEIT et al., 2003; WANNER et al., 2004; LAVERS et al., 2011).

All of the summer events (except for 1890) featured a blocking system over Russia. Furthermore, we identified high pressure ridges over Greece. This supports a meridional evolution and hinders the southeasterly advance of precipitation-producing weather systems. The Azores high, on the western flank of these active weather systems, impedes a zonal evolution with fast system propagations in all types except for ZOF.

Some events show characteristics of more than one type. The event of 1987, classified as CAT, combines a variety of flood-propelling ingredients (e.g., in the fields of precipitation, SLP, vertical velocities, and Θ_e). This indicates that our classification may not withstand an objective categorization, or it may be incomplete. Furthermore, dynamic weather patterns could show key elements of one type and be followed by characteristics of a different type. This is especially likely for similar types (e.g., ECO and CAT, or PCO subtypes).

6 Conclusions

We provide detailed descriptions and analyses of six most severe flood events in Switzerland over the past 150 years. We give an unprecedented three-dimensional view of atmospheric conditions prior to and during extreme floods between 1868 and 1950. This is achieved by combining: (a) traditional sources (e.g., ground measurements), (b) contemporary expert knowledge and documentary information, and (c) novel digitized precipitation data and a new reanalysis data set (20CR). The results are: (i) a detailed verification of the 20CR data set for the six events, (ii) a subjective classification of the flood-triggering weather situations, and (iii) a comprehensive summary of the most important variables.

(i) The long instrumental time series reaching back to 1868 (e.g., discharge, precipitation, and temperature), observational data (e.g., tethered balloon soundings, wind, and snow cover), and historical sources (e.g., reports and assessments by early meteorologists) are used to validate the reanalysis data set. The 20CR data provide plausible synoptic-scale patterns. The wind direction in the 20CR data and the temperature data are in good agreement with the observational data. Precipitation is substantially underestimated in the 20CR ensemble mean. One cause may be the shape and height of the alpine topography in 20CR (e.g., the southern flank of the Alps is convex instead of concave in the model), which leads to a deflection instead of convergence of low-level winds. The exact location and the timing of intense precipitation are often inaccurate. However, the progression of precipitation fields is well captured. Therefore, assessment of smaller scale features (such as terrain-induced flow modulations) requires additional information (e.g., local observations and studies).

(ii) We detected common specific (synoptic) meteorological situations, which can be associated with the floods. These five weather situations ("types") indicate:
- Instability and ascent of air associated with strong temperature and moisture gradients.
- Stationarity of a weather system (e.g., when surrounding highs impede system propagation).
- Repeated episodes of heavy precipitation over a few days, or multiple phases of moisture advection/convection (in a number of events only).

(iii) From a hydrological point-of-view, short-term triggers include rapid warming accompanied by heavy precipitation or continuously warm and rainy spells. Interestingly, precipitation rates during early events exceed those during recent events. Regarding long-term disposition, our results underline the importance of soil saturation (by excessive water supply over several months) ahead of a flood event. One typical pattern is prolonged cool (winter to spring) conditions followed by warm and wet early summer.

In conclusions, our analyses support the findings of previous studies (e.g., PFISTER, 1999), which argue that hydro-meteorological precursors on all time-scales must coincide to produce the most extreme floods in the Alps. This includes hydro-climatological preconditioning, short-term hydrological settings, and the perfect flood-inducing weather patterns (including specific mesoscale flow modulations). Therefore, although a weather situation may resemble a schematic illustration in Fig. 9, it is not guaranteed to trigger a major flood event.

The influence of anomalous temperature (prolonged wintery conditions, warm and rainy spells, rapid warming; see Table 1) implies concerns about the behavior of such flood-setting patterns in a warmer climate. Especially relevant is the role of rapid snowmelt at high elevations (related to sudden thaws and strong winds in the cool seasons). In addition, enhanced evaporation (and atmospheric moisture content) in a warmer atmosphere, and transport over warmer oceans and land surfaces, during the warm seasons merits further analyses.

Acknowledgments

This study is supported by the Swiss National Science Foundation (NCCR Climate project PALVAREX). The Twentieth Century Reanalysis Project dataset is provided by the U.S. Department of Energy, Office of Science Innovative and Novel Computational Impact on Theory and Experiment (DOE INCITE) program, the Office of Biological and Environmental Research (BER), and the National Oceanic and Atmospheric Administration (NOAA) Climate Program. The former group of Christian Pfister, at the History Department, University of Bern, is acknowledged for providing access to the EuroClimHist database. DigiHom is a joint project of the Institute for Atmospheric and Climate Science (IACETH; at the Swiss Federal Institute of Technology) and the Federal Office of Meteorology and Climatology (MeteoSwiss). Mischa Croci-Maspoli is particularly acknowledged for very helpful comments. Jürg Luterbacher was supported by the EU/FP7 project ACQWA (#212250), the Deutsche Forschungsgemeinschaft project PRIME 1 and 2 ('Precipitation in the past millennium in Europe' and Precipitation In past Millennia in Europe - extension back to Roman times') within the Priority Programme INTERDYNAMIK and the project "Climate Change and Extreme Weather in Hesse - Analysis of observation data and ensemble projections for the 21st century" funded by the Hessian Centre on Climate Change and Geology. We are thankful to Monique Stewart who checked and corrected English vocabulary, grammar, and style. Last, but not least, we wish to thank Heini Wernli and Joaquim Pinto for constructive reviews which greatly improved the quality of the article.

References

Ambrosetti, W., L. Barbanti, R. de Bernardi, V. Libera, A. Rolla, 1994: La piena del Lago Maggiore dell'autunno 1993: un evento di portata secolare. – Documenta dell'Istituto Italiano di Idrobiologia. **45**, 49 pp.

Ansell, T. J., P. D. Jones, R. J. Allan, D. Lister, D. E. Parker, M. Brunet, A. Moberg, J. Jacobeit, P. Brohan, N. A. Rayner, E. Aguilar, H. Alexandersson, M. Barriendos, T. Brandsma, N. J. Cox, P. M. Della-Marta, A. Drebs, D. Founda, F. Gerstengarbe, K. Hickey, T. Jonsson, J. Luterbacher, O. Nordli, H. Oesterle, M. Petrakis, A. Philipp, M. J. Rodwell, O. Saladie, J. Sigro, V. Slonosky, L. Srnec, V. Swail, A. M. Garcia-Suarez, H. Tuomenvirta, X. Wang, H. Wanner, P. Werner, D. Wheeler, E. Xoplaki, 2006: Daily mean sea level pressure reconstructions for the European-North Atlantic region for the period 1850 – 2003. – J. Climate. **19**, 2717–2742.

Arpagaus, J., 1870: Die Hochwasser des Jahres 1868 mit besonderer Berücksichtigung des Kantons Graubünden. – Denkblätter, Selbstverlag des Autors.

Aschwanden, H., 2000: Hochwasser 1999, Analyse der Messdaten und statistische Einordnung. – Hydrologische Mitteilungen der Landeshydrologie und -geologie Nr. **28**, 116 pp.

Bardossy, A., F. Filiz, 2005: Identification of flood producing atmospheric circulation patterns. – J. Hydrol. **313**, 48–57.

Begert, M., T. Schlegel, W. Kirchhofer, 2005: Homogeneous temperature and precipitation series of Switzerland from 1864 to 2000. – Int. J. Climatol. **25**, 65–80.

Begert, M., G. Seiz, N. Foppa, T. Schlegel, C. Appenzeller, G. Müller, 2007: Die Überführung der klimatologischen Referenzstationen der Schweiz in das Swiss National Basic Climatological Network (Swiss NBCN). – Arbeitsberichte der MeteoSchweiz. **215**, 43.pp.

Bezzola, G.R., C. Hegg (Ed.), 2007: Ereignisanalyse Hochwasser 2005: Teil 1 - Prozesse, Schäden und erste Einordnung, Bundesamt für Umwelt BAFU, Eidgenössische Forschungsanstalt WSL. – Umwelt-Wissen. **07/07**, 215 pp.

Bezzola, G.R., C. Hegg (Ed.), 2008: Ereignisanalyse Hochwasser 2005: Teil 2 - Analyse von Prozessen, Massnahmen und Gefahrengrundlagen, Bundesamt für Umwelt BAFU, Eidgenössische Forschungsanstalt WSL. – Umwelt-Wissen. **08/25**, 429 pp.

Bezzola, G.R., C. Hegg, A. Koschni (Ed.), 2008: Synthesebericht zur Ereignisanalyse Hochwasser 2005 in der Schweiz. – Eidgenössisches Departement für Umwelt, Verkehr, Energie und Kommunikation UVEK, 22 pp.

Billwiller, R., 1876: Die Niederschläge im Juni 1876 in der Schweiz. – Orell Füssli & Co, Die Eisenbahn, Le chemin de fer 4/5, 6 pp.

Billwiller, R., 1910: Die Niederschläge und Hochwasserkatastrophe vom 14./15. Juni 1910 und ihre Ursachen. – In: Annalen der Schweizerischen Meteorologischen Zentral-Anstalt (ASMA), **47**. Jahrgang, Zürcher und Furrer, Zürich, 7 pp.

Billwiller, R., A. Bühler, 1891: Die forstlich-meteorologischen Stationen. – In: Mittheilungen der Schweizerischen Centralanstalt für das forstliche Versuchswesen, Zürich, **1**, 2/3, 193–200.

Boudevillain, B., S. Argence, C. Claud, V. Durocq, B. Joly, A. Joly, D. Lambert, O. Nuissier, M. Plu, D. Ricard, P. Arbogast, A. Berne, J.P. Chaboureau, B. Chapon, F. Crépin, G. Delrieu, E. Doerflinger, B.M. Funatsu, B.M. Funatsu, P.E. Kirstetter, F. Masson, K. Maynard, E. Richard, E. Sanchez, L. Terray, A. Walpersdorf, 2009: Cyclogenèses et précipitations intenses en région méditerranéenne origines et caractéristiques. – La Météorologie **66**, 18-28.

Brönnimann, S., O. Martius, H. von Waldow, C. Welker, J. Luterbacher, G. P. Compo, P. D. Sardeshmukh, T. Usbeck, 2012: Extreme winds at northern mid-latitudes since 1871. – Meteorol. Z. **21**, 13–27.

Buzzi, A., L. Foschini, 2000: Mesoscale Meteorological Features Associated with Heavy Precipitation in the Southern Alpine Region. – Meteorol. Atmos. Phys. **72**, 131–146.

Cassardo, C., R. Cremonini, D. Gandini, G. Paesano, R. Pelosini, M.W. Qian, 2001: Analysis of the severe flood event of 13 – 16th October 2000 in Piedmont (Italy). – Cuadernos de Investigacion Geografica. Universidad de La Rioja, No. 27, 147–162.

Coaz, J.F., 1869: Die Hochwasser im September und October 1868 im bündnerischen Rheingebiet : vom naturwissenschaftlichen und hydrotechnisch-forstlichen Standpunkt betrachtet. – Engelmann, Leipzig.

Compo, G. P., J. S. Whitaker, P. D. Sardeshmukh, N. Matsui, R. J. Allan, X. Yin, B. E. Gleason, R. S. Vose, G. Rutledge, P. Bessemoulin, S. Brönnimann, M. Brunet, R. I. Crouthamel, A. N. Grant, P. Y. Groisman, P. D. Jones, M. Kruk, A. C. Kruger, G. J. Marshall, M. Maugeri, H. Y. Mok, Ø. Nordli, T. F. Ross, R. M. Trigo, X. L. Wang, S. D. Woodruff, S. J. Worley, 2011: The Twentieth Century Reanalysis Project. – Quart. J. Roy. Meteor. Soc. **137**, 1–28.

Doswell, C. A., H. E. Brooks, R. A. Maddox, 1996: Flash flood forecasting: An ingredients-based methodology. – Wea. Forecast. **11**, 560–581.

Doswell, C. A., C. Ramis, R. Romero, S. Alonso, 1998: A diagnostic study of three heavy precipitation episodes in the western Mediterranean region. – Wea. Forecast. **13**, 102–124.

EuroClimHist; Dietrich-Felber, U. (Ed.), C. Pfister, 2008: EuroClimHist, A Data-Base on past Weather and Climate in Europe and its Human Dimension. – Bern, www.wsu.hist.unibe.ch/index.php?id=190.

Ferguson, C. R., G. Villarini, 2012: Detecting inhomogeneities in the Twentieth Century Reanalysis over the central United States. – J. Geophys. Res. **117**, D05123. Published online March 10th 2012; DOI: 10.1029/2011JD016988.

FORSTER, F., C. HEGG, 2000: Die Hochwasser vom Mai 1999: eine Analyse anhand von hydrologischen Messungen in kleinen Einzugsgebieten. – Schweizerische Zeitschrift für Forstwesen. **151/6**, 183–193.

FREI, C., 2005: August-Hochwasser 2005: Analyse der Niederschlagsverteilung. – MeteoSchweiz.

FREI, C., J. SCHMIDLI, 2006: Das Niederschlagsklima der Alpen: Wo sich Extreme nahe kommen. – Promet 32, 1/2, Meteorologische Fortbildung, Deutscher Wetterdienst.

FREI, C., H. DAVIES, J. GURTZ, C. SCHAER, 2000: Climate dynamics and extreme precipitation and flood events in Central Europe. – Integrated Assessment, Springer, Netherlands **1**, 281–300.

FÜLLEMANN, C., M. BEGERT, M. CROCI-MASPOLI, S. BRÖNNIMANN, 2011: DigiHom - Digitalisieren und Homogenisieren von historischen Klimadaten des Swiss NBCN. – Arbeitsberichte der MeteoSchweiz, **236**, 48 pp.

GODINA, R., P. LALK, P. LORENZ, G., MÜLLER, V. WEILGUNI, 2006: Hochwasser 2005, Ereignisdokumentation. – Teilbericht des Hydrographischen Dienstes BMLFUW, Wien.

GREBNER, D., 1993: Meteorologische Analyse des Unwetters von Brig und Saas Almagell vom 24. September 1993– In: Ursachenanalyse der Hochwasserereignisse. – Bundesamt für Wasserwirtschaft BWW, 4, 23 1993, Geographisches Institut ETH Zürich im Auftrag des Bundesamtes für Wasserwirtschaft BWW, 11 pp.

GREBNER, D, K.G RICHTER, 1991: Gebietsniederschlag, Ereignisanalysen 1987 und Abhängigkeitscharakteristiken. – Mitt. Landeshydrol. und -geologie **14**, 23–40.

GREBNER, D., T. ROESCH, 1998: Flächen-Mengen-Dauer-Beziehungen von Starkniederschlägen und mögliche Niederschlagsgrenzwerte in der Schweiz. – vdf Hochschulverlag AG an der ETH Zürich.

GREBNER, D., T. ROESCH, 1999: Zusammenhänge und Beurteilung der Hochwasserperiode in der Schweiz vom 11. bis 15. Mai 1999. – Wasser, Energie, Luft, **91**, 5/6.

GREBNER, D., H. ASCHWANDEN, U. STEINEGGER, M. ZIMMERMANN, 2000: Charakteristik des Hochwassers vom 9. bis 16. Oktober 2000 auf der Alpensüdseite und im Wallis 2000. – Wasser, Energie, Luft. **92**, 11/12.

HILKER, N., C. HEGG, M. ZAPPA, 2008: Unwetterschäden in der Schweiz 1972–2007 mit besonderer Betrachtung des August-Hochwassers 2005. – Interpraevent 2008. Conference Proceedings. **1**, 99–110.

HOINKA, K. P., C. SCHWIERZ, O. MARTIUS, 2006: Synoptic-scale weather patterns during Alpine heavy rain events. – Quart. J. Roy. Meteor. Soc. **132**, 2853–2860.

JACOBEIT, J., R. GLASER, J. LUTERBACHER, H. WANNER, 2003: Links between flood events in central Europe since AD 1500 and large-scale atmospheric circulation modes. – Geophys. Res. Lett. **30**, 1172.

JACOBEIT, J., A. PHILIPP, M. NONNENMACHER, 2006: Atmospheric circulation dynamics linked with prominent discharge events in Central Europe. – Hydrol. Sci. J. **51**, 946–965.

KALNAY, E., M. KANAMITSU, R. KISTLER, W. COLLINS, D. DEAVEN, L. GANDIN, M. IREDELL, S. SAHA, G. WHITE, J. WOOLLEN, Y. ZHU, A. LEETMAA, R. REYNOLDS, M. CHELLIAH, W. EBISUZAKI, W. HIGGINS, J. JANOWIAK, K. C. MO, C. ROPELEWSKI, J. WANG, R. JENNE, D. JOSEPH, 1996: The NCEP/NCAR 40-Year Reanalysis Project. – Bull. Amer. Meteor. Soc. **77**, 437–471.

KISTLER, R., E. KALNAY, W. COLLINS, S. SAHA, G. WHITE, J. WOOLLEN, M. CHELLIAH, W. EBISUZAKI, M. KANAMITSU, V. KOUSKY, H. van den DOOL, R. JENNE, M. FIORINO, 2001: The NCEP-NCAR 50-year reanalysis. Monthly means CD-ROM and documentation. – Bull. Amer. Meteor. Soc. **82**, 247–267.

KLEIN TANK, A.M.G. et al. (38 co-authors), 2002: Daily dataset of 20th century surface air temperature and precipitation series for the European Climate Assessment. – Int. J. Climatol. **22**, 1441–1453.

LAVERS, D.A, R.P. ALLAN, E.F. WOOD, G. VILLARINI, D.J. BRAYSHAW, A.J. WADE, 2011: Winter floods in Britain are connected to atmospheric rivers. – Geophys. Res. Lett. **38**, L23803. Published online December 6th, 2011, DOI: 10.1029/2011GL049783.

MARSIGLI, C., A. MONTANI, F. NEROZZI, T. PACCAGNELLA, S. TIBALDI, F. MOLTENI, R. BUIZZA, 2001: A strategy for high-resolution ensemble prediction. II: Limited-area experiments in four Alpine flood events. – Quart. J. Roy. Meteor. Soc. **127**, 2095–2115.

MARKOWSKI, P., Y.P. RICHARDSON, 2010: Mesoscale Meteorology in Midlatitudes. – Chichester, Wiley, **407**.

MARTIUS, O., E. ZENKLUSEN, C. SCHWIERZ, H. C. DAVIES, 2006: Episodes of Alpine heavy precipitation with an overlying elongated stratospheric intrusion: A climatology. – Int. J. Climatol. **26**, 1149–116.

MASSACAND, A. C., H. WERNLI, H. C. DAVIES, 1998: Heavy precipitation on the Alpine southside: An upper-level precursor. – Geophys. Res. Lett. **25**, 1435–1438.

MASSACAND, A. C., H. WERNLI, 2001: Influence of upstream diabatic heating upon an Alpine event of heavy precipitation. – Mon. Wea. Rev. **129**, 2822–2828.

MEDINA, S., R. A. HOUZE, 2003: Air motions and precipitation growth in Alpine storms. – Quart. J. Roy. Meteor. Soc. **129**, 345–371.

METEOSWISS, 2006: Starkniederschlagsereignis August 2005. – Arbeitsberichte der MeteoSchweiz. **211**, 63 pp.

PETRASCHECK, A., 1989: Die Hochwasser 1868 und 1987 - Ein Vergleich. – Wasser, Energie, Luft. **81**, 1–3, Baden.

PFISTER, C., 1998: Raum-zeitliche Rekonstruktion von Witterungsanomalien und Naturkatastrophen 1496–1995. – vdf Hochschulverlag AG an der ETH Zürich.

PFISTER, C., 1999: Wetternachhersage: 500 Jahre Klimavariationen und Naturkatastrophen (1496–1995). – Verlag Paul Haupt, Bern.

PFISTER, C., 2009: The "Disaster Gap" of the 20th Century and the Loss of Traditional Disaster Memory. – Gaia. **18**, 239–246.

PFISTER, C., SUMMERMATTER, S., 2004: Katastrophen und ihre Bewältigung : Perspektiven und Positionen. – Haupt Verlag, Bern, Berner Universitätsschriften. **49**, 276.

RÖTHLISBERGER, G., 1991: Chronik der Unwetterschäden in der Schweiz. – Eidgenössische Forschungsanstalt für Wald Schnee und Landschaft Birmensdorf.

RÖTHLISBERGER, G., 1994: Unwetterschäden in der Schweiz im Jahre 1993. – Wasser, Energie, Luft. **86**, 1/2, 1–8.

ROTUNNO, R., R. A. HOUZE, 2007: Lessons on orographic precipitation from the Mesoscale Alpine Programme. – Quart. J. Roy. Meteor. Soc. **133**, 811–830.

RUDARI, R., D. ENTEKHABI, G. ROTH, 2004: Terrain and multiple-scale interactions as factors in generating extreme precipitation events. – J. Hydrometeorol. **5**, 390–404.

RUDARI, R., D. ENTEKHABI, G. ROTH, 2005: Large-scale atmospheric patterns associated with mesoscale features leading to extreme precipitation events in Northwestern Italy. – Adv. Water Resour. **28**, 601–614-61.

SCHMOCKER-FACKEL, P., F. NAEF, 2010: More frequent flooding? Changes in flood frequency in Switzerland since 1850. – J. Hydrol. **381**, 1–8.

SHAPIRO, M.A., D. KEYSER, 1990: Fronts, jet streams and the tropopause. Extratropical Cyclones. – In: The Erik Palmén Memorial Volume, NEWTON, C. W., and E. O. HOLOPAINEN, (Eds.): The Erik Palmén Memorial Volume., Amer. Meteor. Soc. 167–191.

STUCKI, P., J. LUTERBACHER, 2010: Niederschlags-, Temperatur- und Abflussverhältnisse der letzten Jahrhunderte. – Hydrologischer Atlas der Schweiz, Tafel 1.4 (HADES 1.4).

STURM, K., J. GLASER, J. JACOBEIT, M. DEUTSCH, R. BRÁZDIL, C. PfiSTER, J. LUTERBACHER, H. WANNER, 2001: Floods in Central Europe since AD 1500 and their Relation to the Atmospheric Circulation. – Petermann Geogr. Mitt. **148**, 18–27.

TRIGO, I. F., T. D. DAVIES, 2002: Meteorological conditions associated with sea surges in Venice: A 40 year climatology. – Int. J. Climatol. **22**, 787–803.

VAN BEBBER, W. J., 1891: Die Zugstrassen der barometrischen Minima nach den Bahnenkarten der deutschen Seewarte für den Zeitraum 1875–1890. – Meteorol. Z. **8**, 361–366.

WANNER, H., C. BECK, R. BRÁZDIL, C. CASTY, M. DEUTSCH, R. GLASER, J. JACOBEIT, J. LUTERBACHER, C. PFISTER, S. PHOL, K. STURM, P. C. WERNER, E. XOPLAKI, 2004: Dynamic and socioeconomic aspects of historical floods in Central Europe. – Erdkunde. **58**, 1–16.

WEHRY, W., 1967: Hochwasser-Wetterlagen in den Alpen. – In: SCHRAM, K., J.C. THAMS (Red.): Neunte Internationale Tagung für Alpine Meteorologie, Brig und Zermatt, 14.–17. September 1966 – Veröffentlichungender SMA, Nr. 4.

WEINGARTNER, R., M. BARBEN, M. SPREAFICO, 2003: Floods in mountain areas - an overview based on examples from Switzerland. – J. Hydrol. **282**, 10–24.

WETTER, O., C. PFISTER, R. WEINGARTNER, J. LUTERBACHER, T. REIST, J. TRÖSCH, 2011: The largest floods in the High Rhine basin since 1268 assessed from documentary and instrumental evidence. – Hydrol. Sci. J. **56**, 733–758.

WIPPERMANN, F., 1984: Air flow over and in broad valleys: Channeling and counter-current. – Contr. Atmos. Phys. **57**, 92–105.